A STUDY OF HYDRAULIC FRACTURE INITIATION IN TRANSVERSELY ISOTROPIC ROCKS

A Thesis

by

VAHID SERAJIAN

Submitted to the Office of Graduate Studies of
Texas A&M University
in partial fulfillment of the requirements for the degree of

MASTER OF SCIENCE

August 2011

Major Subject: Petroleum Engineering

A Study of Hydraulic Fracture Initiation in Transversely Isotropic Rocks

A STUDY OF HYDRAULIC FRACTURE INITIATION IN TRANSVERSELY ISOTROPIC ROCKS

A Thesis

by

VAHID SERAJIAN

Submitted to the Office of Graduate Studies of
Texas A&M University
in partial fulfillment of the requirements for the degree of

MASTER OF SCIENCE

Approved by:

Chair of Committee,	Ahmad Ghassemi
Committee Members,	Stephen A. Holditch
	Benchun Duan
Head of Department,	Stephen A. Holditch

August 2011

Major Subject: Petroleum Engineering

ABSTRACT

A Study of Hydraulic Fracturing Initiation in Transversely Isotropic Rocks.

(August 2011)

Vahid Serajian, B.S.; M.S., Amirkabir University of Technology (Tehran Polytechnic)

Chair of Advisory Committee: Dr. Ahmad Ghassemi

Hydraulic fracturing of transverse isotropic reservoirs is of major interest for reservoir stimulation and in-situ stress estimation. Rock fabric anisotropy not only causes in-situ stress anisotropy, but also affects fracture initiation from the wellbore. In this study a semi-analytical method is used to investigate these effects with particular reference to shale stimulation. Using simplifying assumptions, equations are derived for stress distribution around the wellbore's walls. The model is then used to study the fracture initiation pressure variations with anisotropy. A sensitivity analysis is carried out on the impact of Young's modulus and Poisson's ration, on the fracture initiation pressure. The results are useful in designing hydraulic fractures and also can be used to develop information about in-situ rock properties using failure pressure values observed in the field. Finally, mechanical and permeability anisotropy are measured using Pulse Permeameter and triaxial tests on Pierre shale.

DEDICATION

To my parents, Mohammadreza Serajian and Mahin Zinsazi and my siblings,

Sanaz and Sahand Serajian, for all their support and help

NOMENCLATURE

a	Radius of the well
a_{ij}	Components of compliance tensor
E, E'	Young's modulus in parallel and perpendicular planes
E_h, E_v	Young's modulus in horizontal and vertical planes, respectively
h_i , h_j	Direction cosines of the i and j axes in relation to the axis of symmetry
H'	Compliance matrix in anisotropy coordination system
I	Imaginary unit
K	Anisotropy ratio, permeability
K_h, K_v	Permeability in horizontal and vertical directions, respectively
l,m,n	Direction cosines of the unit vectors in x, y, z directions respectively
P_w	Mud pressure in the well
P_p	Pore pressure
$\Re e$	Real component of a complex number
α	Biot effective stress coefficient
α_h , α_v	Biot effective coefficient in horizontal and vertical directions
β_{ij}	Reduced strain coefficient

ε_h , ε_H	Strain component in min. and max. principal horizontal stress directions
δ_{ij}	Kronecker delta
ξ	Poro elastic coefficient ($0 < \xi < 1$)
$\mu_i \quad i = 1,2,3$	Characteristic roots of the stress
$\Phi'_i \ , i = 1,2,3$	Derivatives of the stress analytical functions
σ_v	Vertical stress
σ_h	Minimum horizontal stress
σ_H	Maximum horizontal stress
σ_t	Rock tensile strength
σ_{eff}	Effective stress
$\sigma_{xx}, \sigma_{yy}, \sigma_{zz}$	Total normal stresses in Cartesian coordination
$\sigma_{x,o}, \sigma_{y,o}, \sigma_{z,o}$	Original (in-situ) stresses in Cartesian coordination
$\sigma_{x,i}, \sigma_{y,i}, \sigma_{z,i}$	Induced stresses in Cartesian coordination
$\tau_{xy}, \tau_{xz}, \tau_{xy}$	Total shear stresses in Cartesian coordination
$\tau_{xy,o}, \tau_{xz,o}, \tau_{xy,o}$	Original (in-situ) shear stresses in Cartesian coordination
υ, υ'	Poisson's ration in the parallel and perpendicular planes, respectively

υ_h, υ_v	Poisson's ration in horizontal and vertical planes, respectively

TABLE OF CONTENTS

Page

LIST OF FIGURES

Page

Page

LIST OF TABLES

Page

1. INTRODUCTION AND LITERATURE REVIEW

Unconventional petroleum resources are among the most important sources of energy and tend to occur in formations with elastic and hydraulic anisotropy. The different mechanical properties in different directions can cause difficulty in accurately estimating the safe mud weight while drilling and the pressure required for stimulation during fracturing treatment. Consideration of general anisotropy is impractical, but the commonly encountered case of transverse isotropy lends itself to analytical treatment. A transversely isotropy rock is one with mechanical properties that are symmetric about an axis (called axis of rotation). Laminated sedimentary rocks such as shales can be classified as transversely isotropic. Very low permeability is the main constraining factor in gas production from shales so that stimulation from inclined or horizontal wells becomes necessary.

Prediction of fracture initiation pressure in inclined or horizontal wellbores is essential for safe drilling and efficient hydraulic fracture stimulation. To predict the pressure requirements in these activities, the stress distribution around the wellbore should be assessed. This is often achieved using (Kirsch 1898) solution for elastic and isotropic rocks. (Haimson and Fairhurst 1967) proposed analytical equations for stress state around a vertical borehole in elastic rock for estimating the fracturing pressure.

This thesis follows the style of *SPE Journal*.

(Hossain et al. 2000) also estimated the fracture initiation pressure for open hole wells drilled in isotropic rocks with different trajectories. Other equations have also been proposed for stress distribution around a wellbore in anisotropic elastic and poro elastic rock. (Deily and Owens 1969; Hsiao 1988; Jaeger et al. 2007)

Stress analysis assuming isotropy can be inaccurate and often underestimate fracturing pressure (e.g., Suarez-Rivera et al., 2006). (Amadei 1983) and (Lekhnitskii 1963) solved the stress distribution around inclined boreholes in transverse isotropic rocks. Aadnoy (Aadnoy 1988; Aadnoy 1989; Aadnoy and Chenevert 1987) simplified Amadei and Lekhnitskii's methods to estimate the stress distribution around horizontal wells but he neglected the effect of Poisson's ration difference in vertical and horizontal directions for transversely isotropic rocks. His simplified equations may result in erroneous conclusions, especially during back analysis to estimate the in-situ stresses and rock mechanical parameters. Ong et al. (Ong 1994; Ong and Roegiers 1993; Ong and Roegiers 1996) also implemented (Amadei 1983) and (Lekhnitskii 1963) method for wellbore stability and fracture initiation estimation in inclined and horizontal wells. (Abousleiman and Cui 1998) solved the stress distribution around a well in transversely isotropic poroelastic rock drilled perpendicular to the plane of isotropy.

In this study, an analytical technique proposed by (Lekhnitskii 1963) and (Amadei 1983) is used to study the stress distribution around wellbore drilled horizontally in a transversely isotropic formation. The focus is on linear elasticity and the time dependent and plastic behaviors of rock are not considered.

2. GENERAL DEFINITIONS, STRESS AND STRAIN EQUATIONS

2.1 Introduction

A rock mass is subjected to a combination of gravitational and tectonic stresses. Knowledge of the stress distributions is critical in geosciences and geo-engineering projects since it is the most important factor in assessing the stability of the underground openings.

Different rocks with various mechanical properties exist in the nature. The most commonly used procedure in the engineering projects assumes the rock mass as a CHILE[1] rock. Assuming the CHILE rock in real projects does not seems to be the perfect choice in all the cases since anisotropy, heterogeneity and nonlinearity is always seen in all rocks and should be taken into account in real world. Shales are one of the most important examples of such cases that assuming their mechanical properties as isotropic may lead to wrong interpretations in the projects especially in deep reservoirs with high pressures and challenging conditions.

In this section, the mechanical properties of the shales are reviewed and the effects of different foliation, in-situ stress orientation and the wellbore trajectory are studied on the overall compliance matrix of the stress-strain relation. The results will be used for studying the hydraulic fracturing initiation in horizontal wells in shales.

[1] Continuous Homogeneous Isotropic Linearly Elastic

2.2 Basic Definitions

There are some important definitions which should be mentioned before starting the discussions;

- *Elasticity*: A rock is called Elastic when the deformations associated with loading are all recoverable after the unloading.
- *Homogeneity, Heterogeneity*: The rock is called homogeneous if the mechanical properties are identical in different locations and is heterogeneous if these properties vary with the location from point to point.
- *Orthotropic Materials:* A material that possesses different mechanical properties in different orthogonal directions.
- *Isotropy, Anisotropy*: A rock is called isotropic when its mechanical properties don't change with the direction and is called anisotropic when these properties change with direction. Anisotropy is the characteristic of the rocks with long minerals and layered deposition. Shales, schists, slates and bedded sandstones are the most typical anisotropic rocks with layered structure. In case of sandstones, they are usually considered as isotropic but in some of them due to the mixture of clay minerals in the rock mass, existence of micro fracs in some orientations and some other structural characteristics, the behavior of the sandstones cannot be explained by isotropy and should be considered anisotropic.

2.3 Sign Convention

(Jaeger et al. 2007) suggest that in stress and strain analyses in the rocks, compressive stresses should be taken as positive. They mention that the compressive stresses are more common in rock mechanics than the tensile stresses. If we are to use the same sign convention as most other engineering (i.e. mechanical engineering), we should have added a negative sign to all the equations that deal with compressive stresses which finally increases the complexity in the analyses.

In this study:

- Normal stresses are shown with Sigma sign (i.e. σ_{xx})
- Shear stresses are shown with tau sign (i.e. τ_{xy})

The stress notations of the compressive and shear stresses are shown in **Fig. 1**. The coordinate system and the stress directions are also shown accordingly. Since this study is sensitive to the stress direction, knowledge of the sign convention is essential.

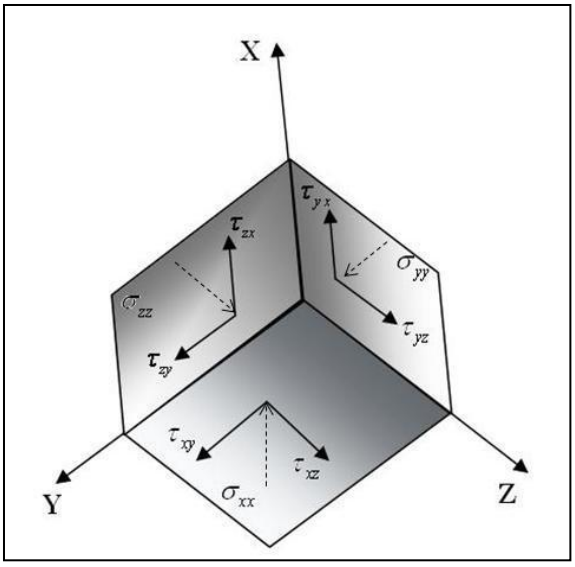

Fig. 1—Three dimensional stress notations.

As can be inferred from **Fig. 1**, the first subscript of the stresses shows the surface which the stress vector acts and the second subscript shows the direction of the stress component. For example, the shear stress τ_{xy} indicates that the stress is in X plane and in Y direction. Other stress components can be explained the same way.

2.4 Constitutive Relations

In engineering, a constitutive equation is a relationship between the stress and strain in a specific material. In other words, constitutive equation can approximate the occurring strain of a material which is under stress. The constitutive equations can be linear, if the deformations are relatively small and can be non-linear in large displacements such as collapses and deteriorations. In this study, since we are dealing

with comparatively small deformations, the linear constitutive equations may be the most reasonable assumption.

To calculate the response of a linear elastic homogeneous and continuous anisotropic rock, generalized hook's law has been used. Generalized Hooke's law is given by:

$$\sigma_{ij} = C_{ijkl}.\ \varepsilon_{kl} \quad \text{..... (2.1)}$$

where σ_{ij} and ε_{kl} denote the stress and strain component, respectively and C_{ijkl} is called the tensor of elastic constants or tensor of compliance. C_{ijkl} has 81 independent components in the most general case but due to the symmetry in stress and strain tensors it can be reduced to 21 components since:

$$\sigma_{ij} = \sigma_{ji}\ ,\ \varepsilon_{kl} = \varepsilon_{lk} \quad \text{..... (2.2)}$$

$$C_{ijkl} = C_{klij} \quad \text{..... (2.3)}$$

$$C_{ijkl} = C_{jikl} \quad \text{..... (2.4)}$$

$$C_{ijkl} = C_{jilk} \quad \text{..... (2.5)}$$

Equation (2.1) can be rewritten as:

$$\varepsilon_{ij} = A_{ijkl}.\sigma_{kl} \quad \text{..... (2.6)}$$

where A_{ijkl} is called the compliance tensor. (Lekhnitskii 1963) used the notation below to show the compliance tensor in its general case:

$$\begin{bmatrix} \varepsilon_x \\ \varepsilon_y \\ \varepsilon_z \\ \gamma_{yz} \\ \gamma_{xz} \\ \gamma_{xy} \end{bmatrix} = \begin{bmatrix} \frac{1}{E_x} & \frac{-\upsilon_{yx}}{E_y} & \frac{-\upsilon_{zx}}{E_z} & \frac{\eta_{x,yz}}{G_{yz}} & \frac{\eta_{x,xz}}{G_{xz}} & \frac{\eta_{x,xy}}{G_{xy}} \\ \frac{-\upsilon_{xy}}{E_x} & \frac{1}{E_y} & \frac{-\upsilon_{zy}}{E_z} & \frac{\eta_{y,yz}}{G_{yz}} & \frac{\eta_{y,xz}}{G_{xz}} & \frac{\eta_{y,xy}}{G_{xy}} \\ \frac{-\upsilon_{xz}}{E_x} & \frac{-\upsilon_{yz}}{E_y} & \frac{1}{E_z} & \frac{\eta_{z,yz}}{G_{yz}} & \frac{\eta_{z,xz}}{G_{xz}} & \frac{\eta_{z,xy}}{G_{xy}} \\ \frac{\eta_{yz,x}}{E_x} & \frac{\eta_{yz,y}}{E_y} & \frac{\eta_{yz,z}}{E_z} & \frac{1}{G_{yz}} & \frac{\mu_{yz,xz}}{G_{xz}} & \frac{\mu_{yz,xy}}{G_{xy}} \\ \frac{\eta_{xz,x}}{E_x} & \frac{\eta_{xz,y}}{E_y} & \frac{\eta_{xz,z}}{E_z} & \frac{\mu_{xz,yz}}{G_{yz}} & \frac{1}{G_{xz}} & \frac{\mu_{xz,xy}}{G_{xy}} \\ \frac{\eta_{xy,x}}{E_x} & \frac{\eta_{xy,y}}{E_y} & \frac{\eta_{xy,z}}{E_z} & \frac{\mu_{xy,yz}}{G_{yz}} & \frac{\mu_{xy,xz}}{G_{xz}} & \frac{1}{G_{xy}} \end{bmatrix} \cdot \begin{bmatrix} \sigma_x \\ \sigma_y \\ \sigma_z \\ \tau_{yz} \\ \tau_{xz} \\ \tau_{xy} \end{bmatrix} \quad \text{..... (2.7)}$$

where:

- E_x, E_y, E_z are Young's moduli along the directions x,y, and z, respectively
- G_{yz}, G_{xz}, G_{xy} are shear moduli for planes parallel to YZ,XZ,XY planes, respectively
- $\upsilon_{yx}, \upsilon_{zx}, \upsilon_{zy}, \upsilon_{xy}, \upsilon_{xz}, \upsilon_{yz}$ are Poisson's ration. If the rock is assumed to be compressed (or stretched) along the axial direction, the ratio of the strain in transverse direction to the strain along axial direction is called Poisson's ration. For example, υ_{xy} indicates Poisson's ration in a plane where there is an axial strain (and axial stress) in X direction and a transverse strain in Y direction. Poisson's ration for this case will be the fraction of strain in Y direction to strain in X direction.

- $\mu_{ij,kl}$ characterizes the shear stress in the plane parallel to "ij-plane" that induces the tangential stress in the plane "kl".
- $\eta_{k,ij}$ is called the "coefficient of mutual influence of the first kind" and shows the stretching/shortening in the direction parallel to the one defined by "ij"
- $\eta_{ij,k}$ is called the coefficient of mutual influence of the second kind. It characterizes the shear stress in the "ij-plane" under the influence of normal stress acting in the k-direction.

Note that components of the compliance matrix are usually shown with a_{ij}. For example in (2.7), we have: $a_{12} = \frac{-\upsilon_{yx}}{E_y}$

The compliance tensor in (2.7) can be simplified using the assumptions below:

$$\frac{\upsilon_{ij}}{E_i} = \frac{\upsilon_{ji}}{E_j} \quad \text{..... (2.8)}$$

$$\frac{\mu_{ik,jk}}{G_{jk}} = \frac{\mu_{jk,ik}}{G_{ik}} \quad \text{..... (2.9)}$$

$$\frac{\eta_{ij,k}}{E_k} = \frac{\eta_{k,ij}}{G_{ij}} \quad \text{..... (2.10)}$$

The last three equations above simplify the compliance tensor as some of elastic constants vanish and the compliance matrix becomes diagonally symmetrical.

2.5 Concept of Transverse Isotropy

A special type of orthotropic materials that possess similar mechanical properties in one plane (called *plane of isotropy* or *plane of symmetry*) and different properties in normal directions to this plane are called transversely isotropic materials. Considering a coordination system XYZ, the X-axis coincides with the axis of elastic symmetry (**Fig. 2**). This axis is called *axis of elastic symmetry of rotation* or *axis of rotation.* A rock that shows this kind of elastic symmetry is called a *transversely isotropic rock*. Most of the layered and deposited rocks are characterized as transverse (transversely) isotropic. **Fig. 2** shows the axis of rotation (X-axis) and isotropic plane (YZ plane).

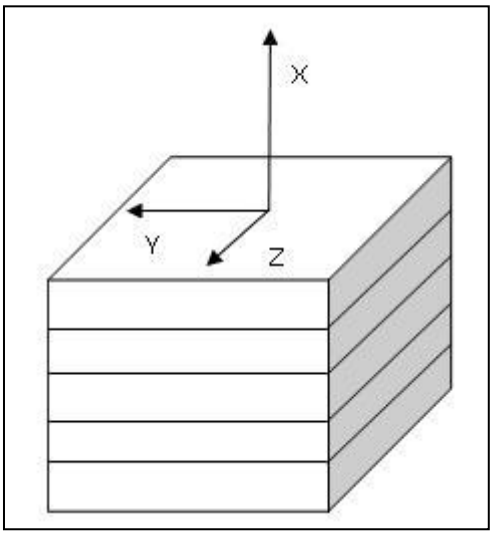

Fig. 2—Axes orientation in a transversely isotropic material.

For rocks with a plane of symmetry as shown in **Fig. 2**, components of (2.7) reduce to:

$$E_y = E_z = E \quad \text{..... (2.11)}$$

$$E_x = E' \quad \text{..... (2.12)}$$

$$\upsilon_{yz} = \upsilon_{zy} = \upsilon \quad \text{.....(2.13)}$$

$$\upsilon_{xz} = \upsilon_{xy} = \upsilon' \quad \text{..... (2.14)}$$

$$G_{yz} = G_{zy} = \frac{E}{2(1+\upsilon)} = G \quad \text{..... (2.15)}$$

$$G_{xz} = G_{xy} = G' \quad \text{..... (2.16)}$$

Among the elastic constants above, the shear modulus G can be expressed in terms of Young's modulus E and Poisson's ration, υ. Therefore, the number of unknowns in a transverse isotropic rock reduces to 5 from total 9 constants in fully anisotropic material.

The shear modulus perpendicular to the plane of isotropy, G' can also be estimated to reduce the complexity in the problem. Several authors (Batugin and Nirenburg 1972; Cauwelaert 1977; Ellefsen et al. 1992) have worked on experimental methods to estimate the shear modulus G' in anisotropic rocks. The relation proposed by (Cauwelaert 1977) is proved to be valid only for rocks with low anisotropy ratio(anisotropy of about 10 percent). (Ellefsen et al. 1992) proposed an experimental procedure for shear modulus estimation in transverse isotropic rocks but their method requires special devices and auxiliary parameters. Among the researches, the relation suggested by (Batugin and Nirenburg 1972) follows relatively simpler analytical

solutions and agrees better with experiments. For example, for Y as the axis of rotation, the shear modulus in the XZ-plane is given by:

$$G' = G_{xz} = \frac{E_x.E_z}{E_x + E_z + 2\upsilon_{xz}.E_z} \quad \text{..... (2.17)}$$

To lower the complexity and simplifying the calculations (2.17) is used in this work to estimate G'. This reduces the number of elastic properties from 5 to 4.

2.6 Pore Pressure and Effective Stress

Pore fluids play an important role in reservoir geomechanics because they support a portion of the total applied stress. Terzaghi's definition of effective stress is:

$$\sigma_{ij}' = \sigma_{ij} - \delta_{ij}.\sigma_p \quad \text{..... (2.18)}$$

where:

σ_{ij}' is the *effective* stress,

σ_{ij} is the total confining stress,

δ_{ij} is the Kronecker delta.

σ_p is the pore pressure.

Biot suggested an "exact" effective stress law as below:

$$\sigma_{ij}' = \sigma_{ij} - \delta_{ij}.\alpha.\sigma_p \quad \text{..... (2.19)}$$

where, α is called "Biot" effective stress coefficient. It varies between 0 and 1 and describes the efficiency of the fluid pressure in counteracting the total applied stress. Its

value depends on the pore geometry and the physical properties of the constituents of the solid system and, hence, on the applied load. For example in sandstones with variable clay content, α changes considerably, but due to the results of (Kwon et al. 2001)in shales with extremely high clay content where there is no stiff rock matrix to support externally applied stresses, it seems that applying the "simple" Terzaghi model (2.18) is more representative.

In this study, hydraulic fracturing initiation pressure has been studied regarding the effective stress law mentioned in (2.18).

2.7 Transformation of Elastic Constants

As seen in (2.6) and (2.7), to define a relation between stress and strain in a material, we require a compliance tensor. In isotropic materials there is no change in rock's mechanical properties with respect to axes of rotation. But in anisotropic materials, since the elastic constants vary from point to point, rotation of the coordination system has a significant effect on the components of the compliance matrix.

To study the effects of different anisotropy orientation and borehole trajectory on compliance tensor, three different coordination systems are required:

- X,Y,Z is the *global* coordination system which in this study is chosen as the orientation of in-situ principal stresses.
- X',Y',Z' is the coordination system attached to the rectilinear anisotropy.
- X_b, Y_b, Z_b is the coordination system attached to the borehole.(local coordination)

The reason to define these three different axes is that the orientation of the plane of rectilinear anisotropy and the borehole trajectory do not necessarily coincide the global orientation. So to transform the stresses in global coordination system (principal stresses) and anisotropic elastic constants in borehole coordination system which we are interested to study, compliance tensor transformation calculations are required.

As mentioned, to find the stress compliance tensor in the generic form, we need to transform the mechanical properties in anisotropy and borehole coordination systems to a unique system such as the global one. Since in this study, the rock layering is assumed to be horizontal, the rectilinear anisotropy coordinate system coincides with the global one, and simplifies the calculations (**Fig. 3**). The matrix transformation calculations have been mentioned in Appendix 1.

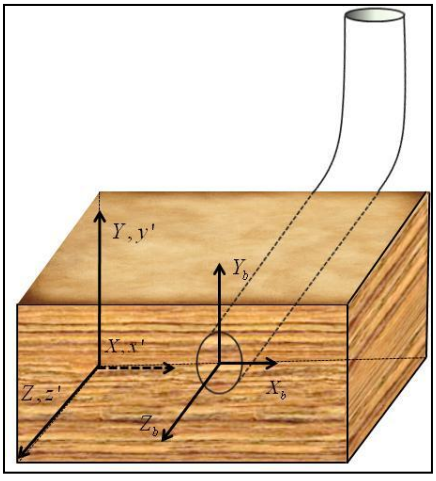

Fig. 3—Position of the horizontal well, local and global coordinate systems attached in a transverse isotropic rock.

As a summary, in this section the basic definitions used in linear poro-elasticity are discussed and introduced and the mechanical properties of the rock in anisotropic (transverse isotropic) rocks are investigated. Also the concept of the compliance tensor and constitutive equations are described and the compliance tensor of the rock mass around the borehole in an anisotropic rock with arbitrary (horizontal) orientation was calculated. The calculated compliance tensor enables us to find the stress distribution around the well at every trajectory from principal stresses and with every different anisotropic characteristic.

3. ANALYTICAL EQUATIONS FOR FRACTURE INITIATION PRESSURE

3.1 Introduction

The objective of this section is to develop an analytical solution for prediction of fracture initiation in a wellbore in transversely isotropic rock (i.e., horizontal drilling through horizontal layers of shales) for different anisotropic ratios. To find the "fracture initiation pressure", the stress distribution around the well should be known. The stress distribution around the well in anisotropic rock is highly dependent on the respective angle of the well orientation with the plane of the transverse isotropy, rock mechanical properties and in-situ stresses. The induced components of the stresses around a wellbore are fist calculated and then added to in-situ stresses to find the total stress around the well. The calculated stress distribution is then used in a failure criterion to estimate the hydraulic fracture initiation pressure.

To simplify the calculation of the stress distributions around the borehole some assumptions are required:

- The rock is a transverse isotropic, in which, the plane of isotropy is horizontal. i.e. a shale reservoir which is horizontally deposited.
- The principal stresses are horizontal and vertical and orthogonal to each other. Or in other words, we will have two principal stresses in horizontal plane and the third principal stress in the vertical plane.

- The drilled horizontal well trajectory can be along minimum/ maximum principal horizontal stress (σ_h or σ_H) or in between them.

The procedure to find the hydraulic fracture initiation pressure is as follows:

- The stress distribution around a horizontal well in transversely isotropic rock should be calculated.
- A proper failure criterion is chosen to assess the fracturing initiation process.
- Since in assessing the stress distribution around the wellbore, the stress distribution depends on the angle and also mud pressure inside the well, at any point around the well, the lowest mud pressure that can satisfy the failure criterion is considered as the fracture initiation pressure and the location in which the lowest satisfying mud pressure has been obtained is considered as the fracture initiation angle.

The general expressions for calculation of the stress distribution around the wellbore are discussed below.

3.2 General Expressions for Calculation of the Stress Functions

To find the stress distributions at any point in an elastic anisotropic rock, five different sets of equations must be satisfied:

1. Equation of Equilibrium
2. Strain- Displacement Relations

3. Compatibility Equations for Strains
4. Constitutive Equations
5. Rocks Boundary Conditions

To find the stress state at any point in an elastic anisotropic rock, we need to use equations 1 to 4 and check the results in the 5th equation (boundary conditions). These sets of differential equations are called "Beltrami-Michell" equations of compatibility for anisotropic rocks it can be written as below:

$$L_4 F + L_3 \psi = 0 \quad \text{..... (3.1)}$$

$$L_3 F + L_2 \psi = 0 \quad \text{..... (3.2)}$$

where:

F and ψ are the stress functions at a point,

And L_2, L_3, L_4 are the linear differential operators and can be calculated as below:

$$L_2 = \beta_{44}\frac{\partial^2}{\partial x^2} - 2\beta_{45}\frac{\partial^2}{\partial x \partial y} + \beta_{55}\frac{\partial^2}{\partial y^2} \quad \text{..... (3.3)}$$

$$L_3 = -\beta_{24}\frac{\partial^3}{\partial x^3} + (\beta_{25} + \beta_{46})\frac{\partial^3}{\partial x^2 \partial y} - (\beta_{14} + \beta_{56})\frac{\partial^3}{\partial x \partial y^2} + \beta_{15}\frac{\partial^3}{\partial y^3} \quad \text{..... ...(3.4)}$$

$$L_4 = \beta_{22}\frac{\partial^4}{\partial x^4} - 2\beta_{26}\frac{\partial^4}{\partial x^3 \partial y} - 2\beta_{16}\frac{\partial^4}{\partial x \partial y^3} + (2\beta_{12} + \beta_{66})\frac{\partial^4}{\partial x^2 \partial y^2} + \beta_{11}\frac{\partial^4}{\partial y^4} \quad \text{..... (3.5)}$$

where:

$$\beta_{ij} = a_{ij} - \frac{a_{i3}.a_{j3}}{a_{33}} \quad (i, j = 1, 2, 4, 5, 6) \quad \text{..... (3.6)}$$

And a_{ij} are components of the compliance tensor, defined in previous section.

If we solve the equations above in terms of F, the equation below is achieved:

$$(L_4 L_2 - L_3^2)F = 0 \quad \text{..... (3.7)}$$

According to (Amadei 1983), $L_3 = 0$ corresponds to the case where there is a plane of elastic symmetry perpendicular to the borehole axis.

According to (Amadei 1983), the algebraic equation that corresponds to equation (3.7) can be written as:

$$l_4(\mu).l_2(\mu) - l_3^2(\mu) = 0 \quad \text{..... (3.8)}$$

where:

$$l_2(\mu) = \beta_{55}\mu^2 - 2\beta_{45}\mu + \beta_{44} \quad \text{..... (3.9)}$$

$$l_3(\mu) = \beta_{15}\mu^3 - (\beta_{14} + \beta_{56})\mu^2 + (\beta_{25} + \beta_{46})\mu - \beta_{24} \quad \text{..... (3.10)}$$

$$l_4(\mu) = \beta_{11}\mu^4 - 2\beta_{16}\mu^3 + (2\beta_{12} + \beta_{66})\mu^2 - 2\beta_{26}\mu + \beta_{22} \quad \text{..... (3.11)}$$

Equation (3.8) always has 6 roots of $\mu_i (i = 1-6)$. (Lekhnitskii 1963) analytically showed that the roots are always purely imaginary and complex and also showed that three of the results are always conjugate roots of three others. So he ignored the conjugate roots and took the first third roots as the answer of the equations. So, to be able to calculate stress distribution in the cases of $L_3 = 0$ we need to calculate $\mu_i (i = 1-3)$.

(Amadei 1983) mentioned 4 different conditions of anisotropy for which the plane of symmetry is perpendicular to the borehole axis and called them “special cases of anisotropy”:

1- Orthotropic material with one elastic symmetry plane perpendicular to the well axis and two other planes parallel to the well axis
2- Transverse isotropy in a plane perpendicular to the well axis
3- Transverse isotropy in a plane striking parallel to the well axis
4- complete isotropy

Fig. 4 and **Fig. 5** show the cases 2 and 3 of the four stress conditions Amadei has mentioned for analytical solutions mentioned above.

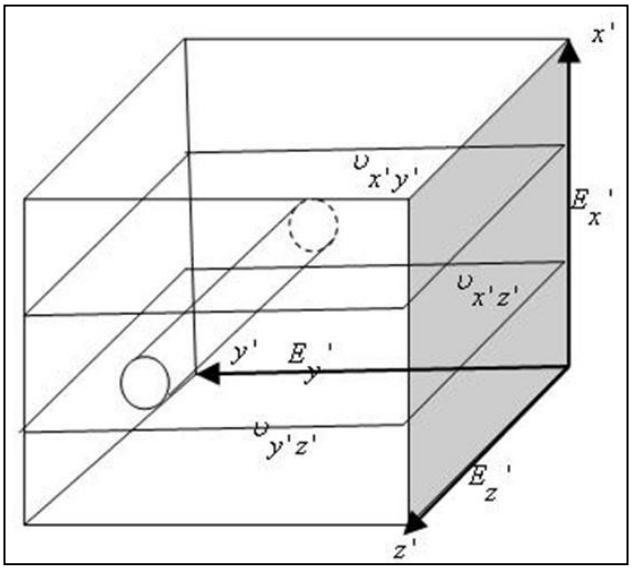

Fig. 4—Transverse isotropy in a plane perpendicular to the well axis.

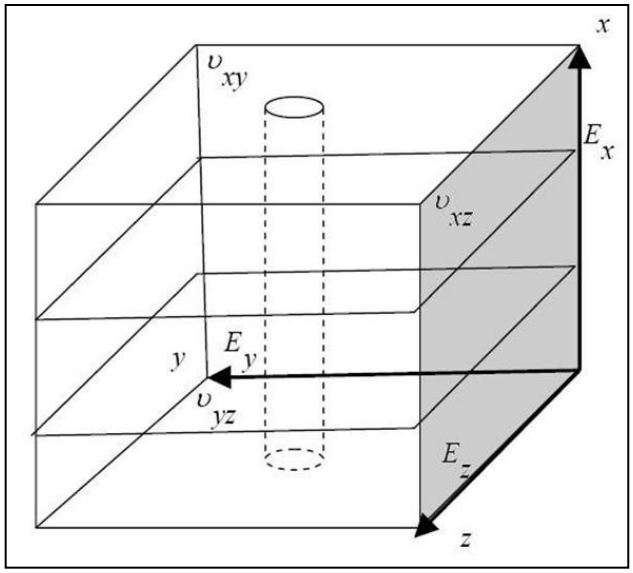

Fig. 5—Transverse isotropy in a plane parallel to the well axis.

Among these 4 cases, case 2 is the one that can model horizontal drilling in a horizontally deposited shale formation. (Ong 1994) used the methods proposed by (Amadei 1983) and (Lekhnitskii 1981) and suggested a series of equations for stress distribution around the wellbore and in this study his contributions will be used.

3.3 Stress State around the Wellbore

Generally, the final state of the stress around a wellbore is sum of the in-situ stress (*original*, $\sigma_{x,o}$) and the stress *induced* by drilling or excavation ($\sigma_{x,i}$). Each of these will affect the total stress distribution; however, we will focus on the induced

stresses in this work and will not discuss the impact of rock anisotropy on the in-situ stress state.

3.3.1 Wellbore Stresses in Transversely Isotropic Rock in Generic Form

The studies to find the stress distribution around a wellbore in an anisotropic rock are done using either analytical or numerical methods. For example, (Suarez-Rivera et al. 2006) used finite element modeling to estimate the stresses around a borehole drilled in transversely isotropic rock and extracted approximate expressions for the tangential stress around the hole. As mentioned before, the analytical approaches are based on the theoretical works of (Lekhnitskii 1981) and (Amadei 1983). Similarly to (Ong and Roegiers 1993) and (Ong 1994), in this study, the analytical work of (Amadei 1983) was used to derive expressions for induced stress distribution around the well and for different borehole orientations of interest.

The total stress components around the wellbore wall are given by (Amadei 1983) as the sum of the original (in-situ) stress (shown by "o" subscript) and a term for an induced component of the stress (shown by "i" subscript) as follows:

$$\sigma_x = \sigma_{x,\,o} + \sigma_{x,\,i} \quad \text{..... (3.12)}$$

$$\sigma_y = \sigma_{y,o} + \sigma_{y,i} \quad \text{..... (3.13)}$$

$$\tau_{xy} = \tau_{xy,o} + \tau_{xy,i} \quad \text{..... (3.14)}$$

$$\tau_{xz} = \tau_{xz,o} + \tau_{xz,i} \quad \text{..... (3.15)}$$

$$\tau_{yz} = \tau_{yz,o} + \tau_{yz,i} \quad \text{..... (3.16)}$$

$$\sigma_z = \sigma_{z,o} + \sigma_{z,i} \quad \text{..... (3.17)}$$

The first term in these equations is the original (in-situ) stress (which should be measured or estimated separately and is assumed known) and the second term is the induced component of the stress.

For induced component of the stresses, (Amadei 1983) proposed:

$$\sigma_{x,\,i} = 2\Re e\left[\mu_1^2\Phi_1'(z_1) + \mu_2^2\Phi_2'(z_2) + \lambda_3\mu_3^2\Phi_3'(z_3)\right] \quad \text{..... (3.18)}$$

$$\sigma_{y,i} = 2\Re e\left[\Phi_1'(z_1) + \Phi_2'(z_2) + \lambda_3\Phi_3'(z_3)\right] \quad \text{..... (3.19)}$$

$$\tau_{xy,i} = -2\Re e\left[\mu_1\Phi_1'(z_1) + \mu_2\Phi_2'(z_2) + \lambda_3\mu_3\Phi_3'(z_3)\right] \quad \text{.....(3.20)}$$

$$\tau_{xz,i} = 2\Re e\left[\lambda_1\mu_1\Phi_1'(z_1) + \lambda_2\mu_2\Phi_2'(z_2) + \mu_3\Phi_3'(z_3)\right] \quad \text{..... (3.21)}$$

$$\tau_{yz,i} = -2\Re e\left[\lambda_1\Phi_1'(z_1) + \lambda_2\Phi_2'(z_2) + \Phi_3'(z_3)\right] \quad \text{.....(3.22)}$$

$$\sigma_{z,i} = -\frac{1}{a_{33}}\left(a_{31}\sigma_{x,i} + a_{32}\sigma_{y,i} + a_{34}\tau_{y,i} + a_{35}\tau_{xz,i} + a_{36}\tau_{xy,i}\right) \quad \text{..... (3.23)}$$

In the above expressions:

- $\Re e$: is real component of an complex expression
- μ_1 is the positive root of the equation:

$$\beta_{55}\mu^2 - 2\beta_{45}\mu + \beta_{44} = 0 \quad \text{.....(3.24)}$$

- μ_2, μ_3 are the positive roots of:

$$\beta_{11}\mu^4 - 2\beta_{16}\mu^3 + (2\beta_{12} + \beta_{66})\mu^2 - 2\beta_{26}\mu + \beta_{22} = 0 \quad \text{..... (3.25)}$$

Equations (3.24) and (3.25) are derived from the sixth order equation, shown in (3.4). The results of μ_i are pure imaginary numbers and half of the roots are conjugates of the other half.

- β_{ij} is called "the reduced strain coefficient" and can be calculated using (3.6)
- a_{ij} are components of the compliance tensor, defined in the previous section.
- λ_i , $i = 1,2,3$ are complex numbers defined by (Amadei 1983)and can be calculated using:

$$\lambda_i = -\frac{l_3(\mu_i)}{l_2(\mu_i)} \quad i = 1,2,3 \quad \text{..... (3.26)}$$

where the functions $l_3(\mu_i)$ and $l_2(\mu_i)$ are introduced in (3.10) and (3.9) respectively

- (Amadei 1983) proposed that the terms Φ'_i , $i = 1,2,3$ are derivatives of the stress functions and are calculated using equations below:

$$\Phi'_1(z_1) = -\frac{1}{2*\Delta*\zeta_1*\sqrt{(\frac{z_1}{a})^2 - 1 - \mu_1^2}}[(i\tau_{xy,o} - \sigma_{yy,o} + P_w)(\mu_2 - \lambda_2\lambda_3\mu_3) + (\tau_{xy,o} - i\sigma_{xx,o} + iP_w)(\lambda_2\lambda_3 - 1) + (\tau_{yz,o} - i\tau_{xz,o})\lambda_3(\mu_3 - \mu_2)] \quad \text{..... (3.27)}$$

$$\Phi'_2(z_2) = -\frac{1}{2*\Delta*\zeta_2*\sqrt{(\frac{z_2}{a})^2 - 1 - \mu_2^2}}[(i\tau_{xy,o} - \sigma_{yy,o} + P_w)(\lambda_1\lambda_3\mu_3 - \mu_1) + (\tau_{xy,o} - i\sigma_{xx,o} + iP_w)(1 - \lambda_1\lambda_3) + (\tau_{yz,o} - i\tau_{xz,o})\lambda_3(\mu_1 - \mu_3)] \quad \text{..... (3.28)}$$

$$\Phi'_3(z_3) = -\frac{1}{2*\Delta*\zeta_3*\sqrt{(\frac{z_3}{a})^2 - 1 - \mu_3^2}}[(i\tau_{xy,o} - \sigma_{yy,o} + P_w)(\lambda_2\mu_1 - \lambda_1\mu_2) + (\tau_{xy,o} - i\sigma_{xx,o} + iP_w)(\lambda_1 - \lambda_2) + (\tau_{yz,o} - i\tau_{xz,o})(\mu_2 - \mu_1)] \quad \text{..... (3.29)}$$

- The complex number Z_i in the above equations is defined as:

$$Z_i = x + \mu_i.y \quad , i = 1,2,3 \quad \text{..... (3.30)}$$

where x and y are the coordinates of the points of interest around the wellbore. In polar coordinate system Z_i can be written as:

$$Z_i = a(\cos\ \theta + \mu_i.\sin\ \theta) \quad \text{..... (3.31)}$$

where $\underline{a}$ is the well radius and θ is the angle measured counterclockwise from the horizontal (x) direction (show in **Fig. 6**).

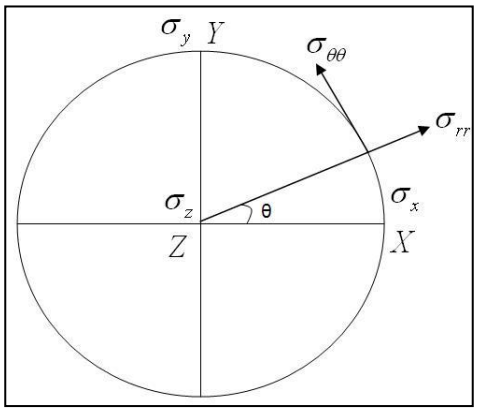

Fig. 6— Transformation around the wellbore from rectangular to polar system.

- For parameters Δ and ζ_i we have:

$$\Delta = \mu_2 - \mu_1 + \lambda_2\lambda_3(\mu_1 - \mu_3) + \lambda_1\lambda_3(\mu_3 - \mu_2) \quad \text{..... (3.32)}$$

$$\zeta_i = \frac{\frac{z_i}{a} + \sqrt{(\frac{z_i}{a})^2 - 1 - \mu_i^2}}{1 - i\mu_i} \quad , i = 1,2,3 \quad \text{..... (3.33)}$$

Using (3.31) and at the wellbore wall (r=a), it can be mathematically shown that:

$$\zeta_i = e^{i\theta} \quad \text{..... (3.34)}$$

If we substitute (3.31) and (3.34) in equations of derivatives of the stress functions eqns. 25-27, we simplified the derivatives of the analytic function $(\Phi_i^{'})$ as below:

$$\Phi_1^{'}(z_1) = A_1[B(\lambda_2\lambda_3 - 1) + C(\mu_2 - \lambda_2\lambda_3\mu_3) + D(\mu_3 - \mu_2)\lambda_3] \quad \text{..... (3.35)}$$

$$\Phi_2^{'}(z_2) = A_2[B(1 - \lambda_1\lambda_3) + C(\lambda_1\lambda_3\mu_3 - \mu_1) + D(\mu_1 - \mu_3)\lambda_3] \quad \text{..... (3.36)}$$

$$\Phi_3^{'}(z_3) = A_3[B(\lambda_2\lambda_3 - 1) + C(\mu_2 - \lambda_2\lambda_3\mu_3) + D(\mu_3 - \mu_2)\lambda_3] \quad \text{..... (3.37)}$$

where:

$$A_i = \frac{1}{2\Delta(\mu_i\cos\theta - \sin\theta)} \quad \text{..... (3.38)}$$

$$B = (p_w - \sigma_{x,o})\cos\theta - \tau_{xy,o}\sin\theta - i[(p_w - \sigma_{x,o})\sin\theta + \tau_{xy,o}\cos\theta] \quad \text{..... (3.39)}$$

$$C = -(p_w - \sigma_{y,o})\sin\theta - \tau_{xy,o}\cos\theta - i[(p_w - \sigma_{y,o})\cos\theta + \tau_{xy,o}\sin\theta] \quad \text{..... (3.40)}$$

$$D = -\tau_{xz,o}\cos\theta - \tau_{yz,o}\sin\theta - i[\tau_{yz,o}\cos\theta - \tau_{xz,o}\sin\theta] \quad \text{..... (3.41)}$$

So in the generic form, to find the stress distribution around a well in an anisotropic (transversely isotropic) rock, a process should be followed and the parameters below should be calculated:

(a) The in-situ stresses are specified. If the wellbore orientation is different from the orientation of the principal stresses, shear stresses also will exist and stress transformation relations (explained in previous section) should be used.

(b) Mechanical properties of the rock (including Young's moduli, Poisson's ration and shear moduli) should be specified in XYZ directions and the compliance tensor should be formed. (according to equation (2.7) in SECTION 2)

(c) Using components of the compliance tensor (a_{ij}) in (2.7) and (3.6), the parameter β_{ij} is calculated.

(d) Using (3.24) and (3.25), the values of β_{ij} (that is already calculated), the values of μ_1, μ_2, μ_3 are calculated.

(e) The $\mu_i,\ i = 1,2,3$ are used in (3.26) to find $\lambda_i,\ i = 1,2,3$

(f) The value of Δ is calculated using (3.32)

(g) The derivatives of the analytic function $(\Phi_i^{'})$ are calculated using eqns. 33-39.

(h) The parameters obtained in (a-g) are finally plugged into eqns. 14-19 to give the induced components of the stresses.

(i) Induced stresses are added to original (in-situ) components of the stresses to give the total stress distribution around the well.

3.3.2 Wellbore Stresses in Transversely Isotropic Rock Drilled along Principal in-situ Stresses

In SECTION 3.3.1, the general solutions for assessment of stress distribution around a horizontal well in horizontally bedded rocks are explained. Since drilling along the in-situ principal stresses is quite common in petroleum industry i.e., for achieving the best fracture shape (longitudinal or transverse fractures), borehole stability issues and minimizing drilling related problems, in this section, the equations mentioned above will be reduced to find the stress distribution around a horizontal well drilled along one principal in-situ stress. The results are then used to estimate the hydraulic fracture initiation pressure around the wellbore in horizontal wells drilled along a principal stress.

By assuming that the horizontal well is drilled along one of the principal horizontal stresses, σ_h or σ_H, the far-filed shear stress components vanish:

$$\tau_{xy,o} = \tau_{yz,o} = \tau_{xz,o} = 0 \quad \text{..... (3.42)}$$

Also, for horizontal wellbores drilled in horizontally laminated transversely isotropic reservoirs, consider that the plane of isotropy is the horizontal plane XZ and the axis of symmetry is the Y-axis. Also, let the principal stresses be vertical and horizontal and aligned with the global coordinate system XYZ and the wellbore is attached to the

local coordination system as shown in **Fig. 7** (Y_b is vertical, while X_b and Z_b are horizontal).

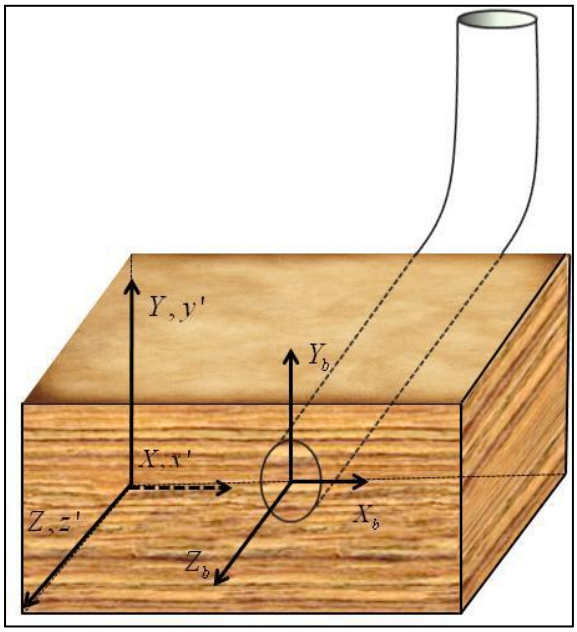

Fig. 7— Horizontal well orientation with respect to 3 coordination systems.

By solving (3.24) and (3.25) for μ_i , $i = 1,2,3$ and substitution in equation 22-24, we get:

$$\lambda_i = 0 \quad , i = 1,2,3 \qquad (3.43)$$

Using (3.43) in (3.32) we get:

$$\Delta = \mu_2 - \mu_1 \qquad (3.44)$$

Also using eqns. 40-42 in eqns. 33-39, we simplified the values for derivatives of the stress analytical functions Φ'_i as follows:

$$\Phi'_1(z_1) = A_1.[-B + C\mu_2] \quad \text{..... (3.45)}$$

$$\Phi'_2(z_2) = A_2.[B - C\mu_1] \quad \text{..... (3.46)}$$

$$\Phi'_3 = 0 \quad \text{..... (3.47)}$$

where A_i is defined in (3.38) and B, C have been simplified to:

$$B = (p_w - \sigma_{x,o})\cos\theta - i[(p_w - \sigma_{x,o})\sin\theta] \quad \text{..... (3.48)}$$

$$C = -(p_w - \sigma_{y,o})\sin\theta - i[(p_w - \sigma_{y,o})\cos\theta] \quad \text{..... (3.49)}$$

By applying the solutions and simplification mentioned in eqns. 42-47, the stress distribution on a wellbore along the principal stresses can be calculated as illustrated in eqns. 48-53. Assuming that the wells have been drilled along maximum horizontal stress, the X, Y and Z directions should be along the σ_v, σ_h and σ_H stresses, respectively.

For total stresses we will have:

$$\sigma_x = \sigma_{x,o} + \sigma_{x,i} = \sigma_v + 2\Re e\left[\mu_1^2\Phi'_1(z_1) + \mu_2^2\Phi'_2(z_2)\right] \quad \text{..... (3.50)}$$

$$\sigma_y = \sigma_{y,o} + \sigma_{y,i} = \sigma_h + 2\Re e\left[\Phi'_1(z_1) + \Phi'_2(z_2)\right] \quad \text{..... (3.51)}$$

$$\sigma_z = \sigma_H - \frac{1}{a_{33}}\left(a_{31}\sigma_{x,i} + a_{32}\sigma_{y,i}\right) \quad \text{..... (3.52)}$$

$$\tau_{xy} = \tau_{xy,i} = -2\Re e\left[\mu_1\Phi'_1(z_1) + \mu_2\Phi'_2(z_2)\right] \quad \text{..... (3.53)}$$

$\tau_{xz} = 0$ ..... (3.54)

$\tau_{yz} = 0$ ..... (3.55)

In these equations, the subscripts "i" and "o" stand for induced and original components of the stresses, respectively.

The stress values are in Cartesian coordination should be converted to polar coordination to be used in borehole geometry. It will be assessed more in SECTION 4.

3.4 Assessment of a Proper Failure Criterion for Fracturing Analysis

Different failure criteria are used to assess the hydraulic fracturing initiation. These criteria are for shear and tensile failure criteria. Shear failure is more common in wellbore stability analysis. However, tensile strength seems to be the best type of criterion for assessing the hydraulic fracture initiation in the wells since rocks have much lower tensile strength than shear strength, so they can break in tension easily. (Daneshy 1973) in his paper presented a criterion for tensile fracturing in an inclined well where the borehole axis has an angle with the orientation of the principal stresses. He considered the effects of the fluid invasion inside the permeable zone on the variation of the induced stresses. But his solution was for isotropic and so not applicable to anisotropy. (Hossain et al. 2000) also studied the hydraulic fracture initiation pressure in inclined wells but he also considered the rock as isotropic.

In this study, after finding the stress distribution around a wellbore in transversely isotropic rock, tensile strength criterion was used to assess the breakdown pressure in the wells.

Tensile failure criterion of the rock states that the fracture initiates where and when the effective tangential stress magnitude equals to rocks tensile strength. In other words:

$$\sigma_\theta - P_p = -\sigma_t \quad \text{..... (3.56)}$$

For simplicity, one can assume that the pore pressure at the wall equals the mud pressure (p_w). By calculating the wellbore pressure (p_w) that satisfies the tensile strength criterion, the location and position of fracture initiation around the well can be estimated. Fracture initiation pressure is the pressure at which p_w overcomes the tangential stress at the wellbore's *weakest point*. Since the hoop (tangential) stress is dependent on the angle, to find the weakest point around the well, (3.56) should be checked for all angles between 0 to 360 degrees, each yielding a different value of p_w pressure. Then, the minimum value of p_w is the fracturing pressure (breakdown pressure) at the *weakest* point around the well which is the fracture initiation point (point of lowest hoop stress).

As mentioned above, to find the breakdown pressure (p_{w_b}), first the tangential stress or σ_θ which is function of the mud pressure inside the well (p_w) is calculated. Since the pore pressure and the rock tensile strength are already known, the critical mud pressure that can satisfy the equation above (the breakdown pressure) can be calculated.

So, as the summary, in this section the general procedure for calculation of stress distribution around a horizontal well drilled inside a horizontally bedded transversely isotropic rock was explained. Also the equations are simplified for the case of a horizontal well drilled along maximum horizontal stress ($\sigma_{H\max}$). At the end, to validate the proposed equations, the anisotropic solution was used to find the stress distribution for a nearly isotropic rock and the results are compared with classic isotropic solutions proposed by Kirsch and a perfect match was reported. In next section, the stress distribution equations will be used to find the breakdown pressure in rocks with different anisotropy ratios.

3.5 Estimation of Fracture Initiation Pressure

Fracture initiation pressure is an important parameter in petroleum industry since it is used in pre-drilling analysis, wellbore stability, and safe mud weight design and should be known to avoid drilling problems such as ballooning, lost circulation and so on. As mentioned in the literature review, many different equations have been proposed to help estimate the formation fracturing pressure before drilling. One of the most common equations is the equation proposed by (Hubbert and Willis 1957). They used the linear isotropic assumption and assumed the well as vertical. In this study our results will be compared with the results of (Hubbert and Willis 1957). Their proposed equation for fracture initiation pressure in a vertical well is as follows:

$$P_b = 3\sigma_h - \sigma_H - \sigma_p + \sigma_t \quad (3.57)$$

Since in horizontal wells, the maximum and minimum in-plane stresses are different from vertical wells, equation of (Hubbert and Willis 1957) is applied to a horizontal well drilled along $\sigma_{H\max}$ as follows:

$$P_b = 3\sigma_h - \sigma_v - \sigma_p + \sigma_t \quad \text{..... (3.58)}$$

Equation (3.58) will be used in next sections to verify the results of fracture initiation pressure with anisotropic solutions.

4. CALCULATION OF FRACTURE INITIATION PRESSURE IN A HORIZONTAL WELL DRILLED IN SHALE

4.1 Introduction

In SECTIONS 1 to 3, the basics of anisotropy, analytical solutions for calculation of stress distribution around the well in different orientations and proper failure criterion for fracturing purposes are explained. In this section, using the equations mentioned in previous sections, the isotropic solutions are compared with anisotropic ones to validate the proposed equations. Numerical examples are solved to show the applications of the proposed equations. Sensitivity analysis is also carried out to assess the effects of anisotropy (Young's modulus and Poisson's ration) on fracture initiation pressure.

4.2 Numerical Example to Find Tangential Stress around the Well

In this section a numerical example is shown to illustrate the procedure for calculation of the tangential stress in horizontal wells. Since the case of drilling along the principal stresses comparatively requires fewer calculations, it was chosen as the numerical example. Consider a horizontal well in shale under an in-situ stress and mechanical properties given in **Table 1** and **Table 2** for a depth of 10,000 ft. (3048 m) and **Table 1** shows available in-situ stresses and rock mechanical properties for calculations.

Table 1—Available in-situ Stresses and Mechanical Properties for Calculations

$\sigma_y=\sigma_v$	$\sigma_x=\sigma_h$	$\sigma_z=\sigma_H$	σ_p	σ_t
psi/ft	**psi/ft**	**psi/ft**	**psi/ft**	**psi**
pa/m	**pa/m**	**pa/m**	**pa/m**	**Mpa**
1	0.8	0.85	0.61	100
($22.6x10^3$)	($18.09x10^3$)	($19.23x10^3$)	($13.79\ x10^3$)	(0.69)

Fig. 8 shows the coordination systems and in-situ stresses at the depth of 10,000 ft. (3048 m).

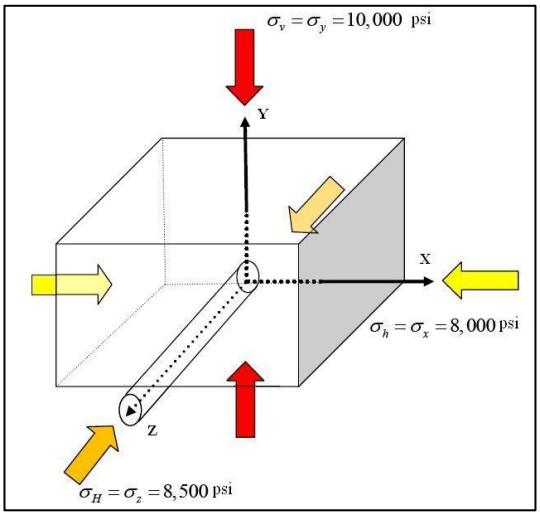

Fig. 8— Well position with respect to in-situ stresses and the coordination system.

In this example, the mechanical properties used in the calculations are chosen close to each other to make the rock *nearly* isotropic. The fracture initiation angle and pressure are calculated using transversely isotropic solutions. They are then compared with isotropic solutions. This step can be considered as the *verification* of the transversely isotropics solution as well. It should be noted that *nearly* isotropic material properties are used and not the exactly isotropic because in the later case, the anisotropic solution fails. Because using exactly similar rock mechanical properties results $\mu_1 = -i$ and $\mu_2 = \mu_3 = i$ in (3.24) and (3.25). Now if the results of $\Phi_i^{'}, i = 1,2$ are calculated using equations (3.45) and (3.46) and used in equations (3.50) and (3.51), it can be seen that the right hand side expression which denotes the induced component of the stresses, is zero. Therefore, using exact rock mechanical properties causes wrong total stress values along X and Y directions.

Table 2—Mechanical Properties of the Rock Used to Validate the Solutions

$E_{hor}=E_x=E_z$ (psi)	$E_{vert}=E_y$ (psi)	Gyz=Gxy (psi)	Gxz (psi)	$\nu_{hor}=\nu_{xz}$	$\nu_{vert}=\nu_{yz}=\nu_{xy}$
1.40001×10^6	1.4×10^6	5.60002×10^5	5.60008×10^5	0.24999	0.25

The compliance tensor of the rock with properties in **Table 2** is:

$$\begin{bmatrix} \frac{1}{E_x} & \frac{-\upsilon_{yx}}{E_y} & \frac{-\upsilon_{zx}}{E_z} & 0 & 0 & 0 \\ \frac{-\upsilon_{xy}}{E_x} & \frac{1}{E_y} & \frac{-\upsilon_{zy}}{E_z} & 0 & 0 & 0 \\ \frac{-\upsilon_{xz}}{E_x} & \frac{-\upsilon_{yz}}{E_y} & \frac{1}{E_z} & 0 & 0 & 0 \\ 0 & 0 & 0 & \frac{1}{G_{yz}} & 0 & 0 \\ 0 & 0 & 0 & 0 & \frac{1}{G_{xz}} & 0 \\ 0 & 0 & 0 & 0 & 0 & \frac{1}{G_{xy}} \end{bmatrix} = \quad \text{.....(4.1)}$$

$$\begin{bmatrix} 7.142806*10^{-7} & -1.78571*10^{-7} & -1.78563*10^{-7} & 0 & 0 & 0 \\ -1.785701*10^{-7} & 7.142857*10^{-7} & -1.785701*10^{-7} & 0 & 0 & 0 \\ -1.785630*10^{-7} & -1.785714*10^{-7} & 7.142806*10^{-7} & 0 & 0 & 0 \\ 0 & 0 & 0 & 1.785709*10^{-6} & 0 & 0 \\ 0 & 0 & 0 & 0 & 1.78568*10^{-6} & 0 \\ 0 & 0 & 0 & 0 & 0 & 1.785709*10^{-6} \end{bmatrix}$$

The matrix Beta can then be calculated using the compliance tensor in (4.1) and (3.6):

$$\beta_{ij} = \begin{bmatrix} 6.69641*10^{-7} & -2.23212*10^{-7} & 0 & 0 & 0 & 0 \\ -2.232109*10^{-7} & 6.69643*10^{-7} & \textit{undefined} & 0 & 0 & 0 \\ \textit{undefined} & \textit{undefined} & \textit{undefined} & 0 & 0 & 0 \\ 0 & 0 & 0 & 1.785709*10^{-6} & 0 & 0 \\ 0 & 0 & 0 & 0 & 1.785687*10^{-6} & 0 \\ 0 & 0 & 0 & 0 & 0 & 1.785709*10^{-6} \end{bmatrix} \text{..... (4.2)}$$

In equation above, the components a_{i3} and a_{3i} , $i = 1,2,3$ are undefined since equation (3.6) is not defined for $i, j = 3$ because it causes a zero value for β_{ij} in equation (3.6) which makes equation 3.9 to 3.11 unsolvable.

Using (3.24) and (3.25) (in SECTION 3) and the values of β_{ij} (already calculated in (4.2)), the values of μ_1, μ_2, μ_3 are calculated.

$$(\mu_1, \mu_2, \mu_3) = (0.999995i\ , 1.0000057i\ , 1.0000061i) \quad \text{..... (4.3)}$$

According to SECTION 3, $\lambda_i = 0,\ i = 1,2,3$ ..... (4.4)

Also $\Delta = \mu_2 - \mu_1 = 0.000010391i$ ..... (4.5)

$\Phi_i^{'}(z_i),\ i = 1,2,3$ is calculated using equations 36 and 43-47 in SECTION 3. Before calculation of $\Phi_i^{'}(z_i)$, we need to calculate the parameters A_i, B, C as below:

$$A_i = \frac{1}{20.782 * 10^{-6} i * (\mu_i \cos\theta - \sin\theta)} \quad \text{..... (4.6)}$$

$$B = (p_w - 8 * 10^3)\cos\theta - i[(p_w - 8 * 10^3)\sin\theta] \quad \text{..... (4.7)}$$

$$C = -(p_w - 10^4)\sin\theta - i[(p_w - 10^4)\cos\theta] \quad \text{..... (4.8)}$$

Using eqns. 43-45 (in SECTION 3) and after calculating variables A_i, B, C for calculation of $\Phi_i^{'}(z_i)$ and after some mathematical simplifications we have:

$$\Phi_1^{'}(z_1) = e^{-2i\theta}(9.624 \times 10^7 - 0.27750\ p_w) \quad \text{..... (4.9)}$$

$$\Phi_2^{'}(z_2) = e^{-2i\theta}(-9.624 \times 10^7 - 0.22250\ p_w) \quad \text{..... (4.10)}$$

$$\Phi_3^{'}(z_3)=0 \quad \text{..... (4.11)}$$

So by plugging the above mentioned variables in eqns. 48-49 (in SECTION 3) we will get:

$$\sigma_x = 8\times10^3 + 2\Re e[e^{-2i\theta} + \frac{p_w}{2}] \quad \text{..... (4.12)}$$

$$\sigma_y = 10^4 + 2\Re e[e^{-2i\theta}(5000 - \frac{p_w}{2})] \quad \text{..... (4.13)}$$

And using (3.53) in SECTION 3 for τ_{xy} calculations we have:

$$\tau_{xy} = p_w \times \Re e[\sin 2\theta] \quad \text{..... (4.14)}$$

Now that all the required variables are calculated, the hoop stress (σ_θ) for the case of a *nearly* isotropic rock can be found using equation below:

$$\sigma_\theta = \sin^2\theta.\ \sigma_x + \cos^2\theta\ .\sigma_y - \sin 2\theta.\ \tau_{xy} - 2p_p + \sigma_t \quad \text{.....(4.15)}$$

Equation above is calculated using a simple conversion from Cartesian to polar coordination system.

As seen above, the equations are functions of the angle around the well (θ) and the mud pressure inside the well (p_w). In the next section, as an example, the hydraulic fracture initiation pressure is calculated using anisotropic solutions and the results are compared with the classic isotropic solutions.

4.3 σ_θ Comparison around the Well Using Isotropic and Anisotropic Solutions

(Kirsch 1898) proposed a set of equations to calculate the stress distribution around a vertical well. Using (Kirsch 1898) equations and by changing the vertical well assumption to horizontal well (by changing the term σ_H to σ_v as the maximum in-plane stress in normal fault regime zones) and some simple mathematical manipulations, the tensile stress distribution around a horizontal well can be calculated as follows:

$$\sigma_\theta = \frac{1}{2}(\sigma_v + \sigma_h - 2P_p)(1+\frac{a^2}{r^2}) - \frac{1}{2}(\sigma_v - \sigma_h)(1+\frac{3a^4}{r^4})\cos 2\theta - \frac{\Delta p * a^2}{r^2} + \sigma_t \quad \text{..... (4.16)}$$

At wellbore wall r=a , and it simplifies to:

$$\sigma_\theta = \sigma_h + \sigma_v - 2(\sigma_v - \sigma_h)\cos 2\theta - 2P_p + \sigma_t \quad \text{..... (4.17)}$$

Since due to the maximum tensile strength criterion, the fracturing initiates at the point with the minimum hoop (tangential) stress values, therefore, the fracture initiates in a horizontal well at the points with minimum tangential stress as below:

$$\sigma_{\theta_{\min}} = 3\sigma_h - \sigma_v - 2P_p - \Delta p + \sigma_t \quad \text{..... (4.18)}$$

where Δp shows the pressure difference between the mud weight and pore pressure. Using the input examples mentioned in **Table 1** and **Table 2** in **Fig. 9** the tangential stress is calculated with isotropic and anisotropic solutions and is compared to each other. These calculations are done with assuming the mud pressure of 8000 psi.

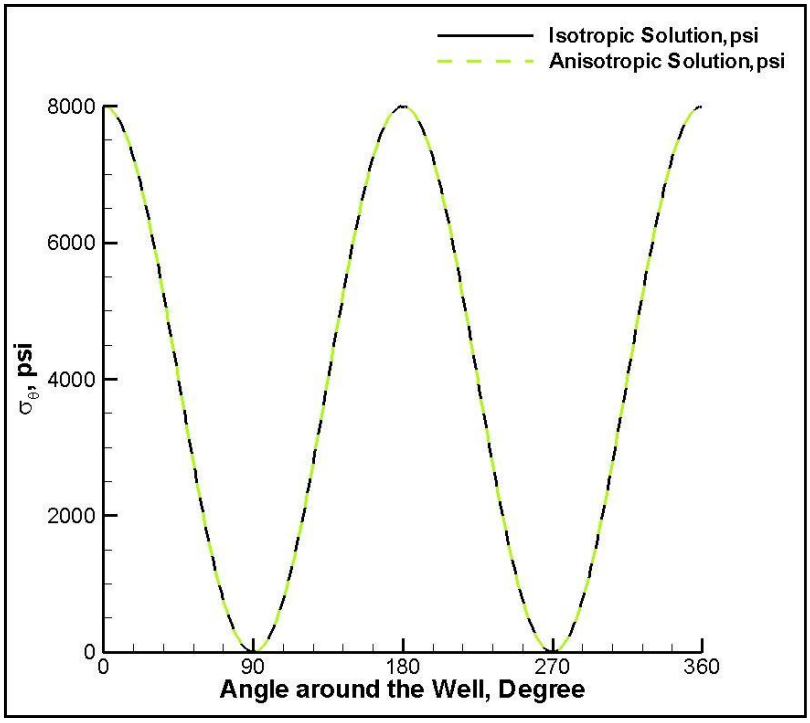

Fig. 9—σ_θ distribution around a nearly isotropic horizontal well drilled along $\sigma_{H\max}$ and with mud pressure of 8000 psi using isotropic and anisotropic solutions.

As can be seen in figure above, at $\theta = 90°, 270°$ which coincides the orientation of the maximum in-plane stress (upper most and lower most points of the well), the tensile strength has its minimum value and is the weakest point around the well for tensile fracturing. So at 8000 psi mud pressure inside the well, the tangential stress goes to tension at $\theta = 90°, 270°$ and the fracture initiates at these two points.

Fig. 9 shows how well the results of isotropic and anisotropic solutions match with each other for a nearly isotropic rock and can be considered as the validation of the solutions.

4.4 σ_θ Comparison around the Well Using Different Anisotropy Ratios

In this section, to show how rock anisotropy can change the stress distribution around the well, three cases of Young's modulus anisotropy are selected and the tangential stress distributions around the well in these three cases are compared. In these cases only the effects of Young's modulus have been studied and the Poisson's ration was assumed isotropic since it is assumed that Poisson's ration doesn't contribute significantly on changing the hoop stress around the well.

These cases are:

1. A *nearly* isotropic case, where $\frac{E_{hor}}{E_{vert}} \approx 1$
2. Anisotropic case where $\frac{E_{vert}}{E_{hor}} = 1.6$
3. Anisotropic case where $\frac{E_{hor}}{E_{vert}} = 1.6$

Fig. 10 shows the tangential stress distribution around the well for cases 1 to 3 mentioned above. In these cases, the mud pressure inside the well is assumed to be 8000 psi.

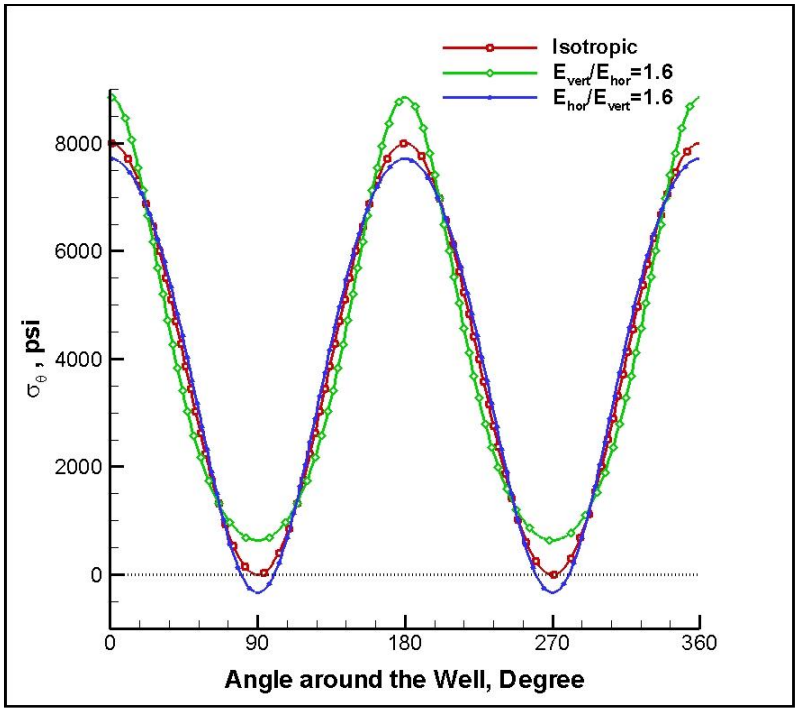

Fig. 10—Tangential stress distribution around the well for three cases with different anisotropy ratios.

As can be seen in figure above, at 8000 psi mud pressure, the isotropic rock ($\frac{E_{hor}}{E_{vert}} \approx 1$or case 1) is about to fail at 90 and 270 degrees since at these two points, the tangential stress curves have zero values. For case 2 where $\frac{E_{vert}}{E_{hor}} = 1.6$, the tangential stress increases and the tensile fracture can't initiate in this case. In other words, to initiate the tensile fracture in case of $\frac{E_{vert}}{E_{hor}} = 1.6$, we require the mud pressure slightly more than 8000 psi.

For case 3 where $\frac{E_{hor}}{E_{vert}} = 1.6$, as can be seen in **Fig. 10**, the tangential stress has gone to tension since its values has become negative in a big zone. Therefore, at 8000 psi mud pressure, the fracture has already been initiated in this case. So, it is obviously seen that Young's modulus anisotropy can increase or decrease the minimum hoop stress- the parameter that plays a key role in hydraulic fracture initiation.

4.5 Estimation of Fracture Initiation Pressure in Horizontal Wells Drilled in Horizontally Deposited Rock

In this section, the effect of different rock properties (different Young's modulus and Poisson's ration) on changing the value of the fracturing initiation pressure is discussed. The in-situ stress conditions are similar to the case introduced in **Table 1** in SECTION 3. Rock mechanical properties used for calculations are also mentioned below in **Table 3**. It is assumed that the well is drilled along maximum horizontal stress ($\sigma_{H\max}$) direction.

A sensitivity analysis was carried out to show how variations in rock mechanical properties change the values of fracture initiation pressure.

As can be seen in **Table 3**, the Young's modulus and Poisson's ration in vertical direction was assumed constant ($E_{vert} = 1.4\times10^6$ and $\upsilon_{vert} = 0.2$) and then Young's modulus in horizontal direction changes between $0.5\times E_{vert} < E_{hor} < 3\times E_{vert}$ and the Poisson's ration in horizontal direction between $0.05 < \upsilon_{hor} < 0.45$.

Due to equation $G = \frac{E}{2(1-\upsilon)}$ in the isotropic (horizontal) plane, assuming Poisson's ration as constant, there is a linear relationship between Young and shear moduli and by changing $0.5 \times E_{vert} < E_{hor} < 3 \times E_{vert}$, the shear moduli will also change to $0.5 \times G_{vert} < G_{hor} < 3 \times G_{vert}$

Table 3—Mechanical Properties of the Rock Being Used for Sensitivity Analysis

$E_{vert}=E_y$ (psi)	$E_{hor}=E_x=E_z$ (psi)	$G_{yz}=G_{xy}$ (psi)	G_{xz} (psi)	$\nu_{hor}=\nu_{xz}$ (fraction)	$\nu_{vert}=\nu_{yz}=\nu_{xy}$ (fraction)
1.4×10^6	$(0.5\text{-}3) \times 1.4 \times 10^6$	5.6×10^5	$(0.5\text{-}3) \times 5.6 \times 10^5$	(0.05-0.45)	0.2

Table 4 shows some numerical examples of how Young's modulus and Poisson's ration can change the value of fracturing pressure in a horizontal well drilled along the maximum horizontal stress direction. 6 numerical examples are shown in **Table 4** with different Young's modulus and Poisson's ration values. As can be seen, the value of fracturing pressure when $\frac{E_{hor}}{E_{vert}} = \frac{\upsilon_{hor}}{\upsilon_{vert}} = 1$ equals to 8000 psi which matches with results of isotropic calculations (equation (3.58)) where:

$$P_b = 3\sigma_h - \sigma_v - \sigma_p + \sigma_t = 3 \times 8000 - 10000 - 6100 + 100 = 8000 \text{ psi} \quad \text{..... (4.19)}$$

Depending on the Young's modulus and Poisson's rations, the fracture initiation pressure can be more or less than the fracturing pressure in isotropic case. For example, when Young's modulus is $\frac{E_{hor}}{E_{vert}} = 0.5$ and Poisson's ration is $\frac{\upsilon_{hor}}{\upsilon_{vert}} = 1$, the fracturing pressure changes from 8000 psi in isotropic to 8877 psi in transversely isotropic rock.

Table 4—Numerical Example to Show Variations of Fracturing Pressure with Different Young's Modulus and Poisson's Ration

Poisson Ratio \ Young's Modulus		$\frac{E_{hor}}{E_{vert}}$		
		0.5	1	1.5
$\frac{\upsilon_{hor}}{\upsilon_{vert}}$	0.5	8845 psi	8030 psi	7650 psi
	1	8877 psi	8000 psi	7726 psi
	1.5	8914 psi	8153 psi	7835 psi

To further study the effects of anisotropy on fracturing pressure, 3000 data points are created using different combinations of Young's modulus ratio $\frac{E_{hor}}{E_{vert}}$ and Poisson's ration $\frac{\upsilon_{hor}}{\upsilon_{vert}}$. These points are selected using the criteria defined in **Table 1**.

The selected data points are then used in the proposed analytical solutions mentioned in SECTION 3.3.1 and 3.3.2 to find the stress distribution around the well and finally the required mud pressure to initiate the first tensile fracture (fracture initiation pressure) was calculated separately for each case. The calculated fracture

initiation pressures are plotted in **Fig. 11** and **Fig. 12** for the wells drilled along $\sigma_{H\max}$ and $\sigma_{h\min}$ respectively. These plots show the variations in fracturing pressure caused by changes in the mechanical properties.

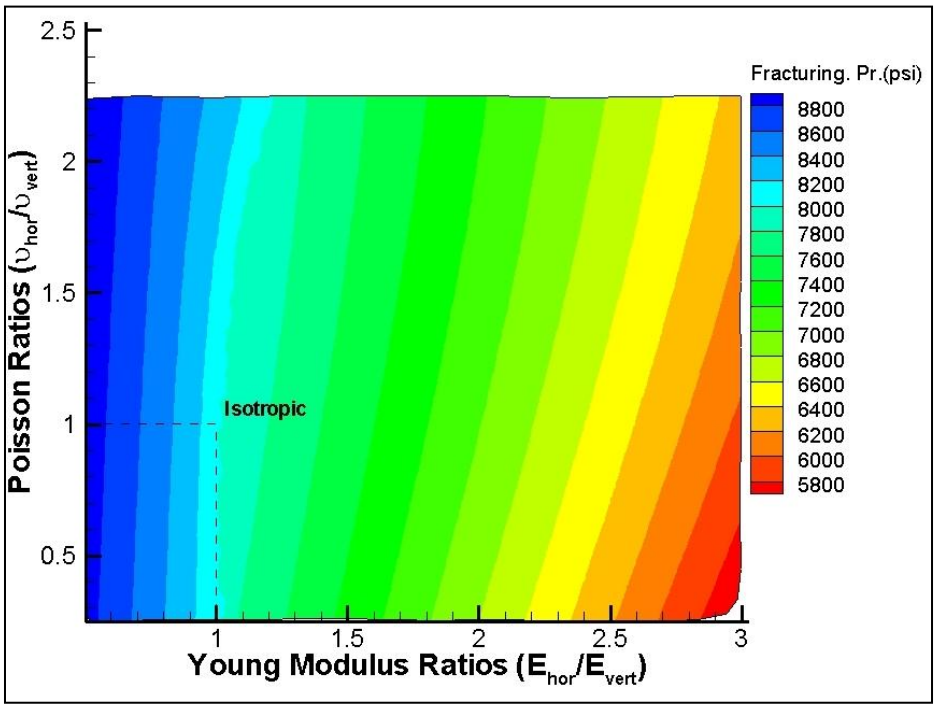

Fig. 11— Fracturing pressure variations in a well drilled along $\sigma_{H\max}$ by changing Young's modulus and Poisson's rations.

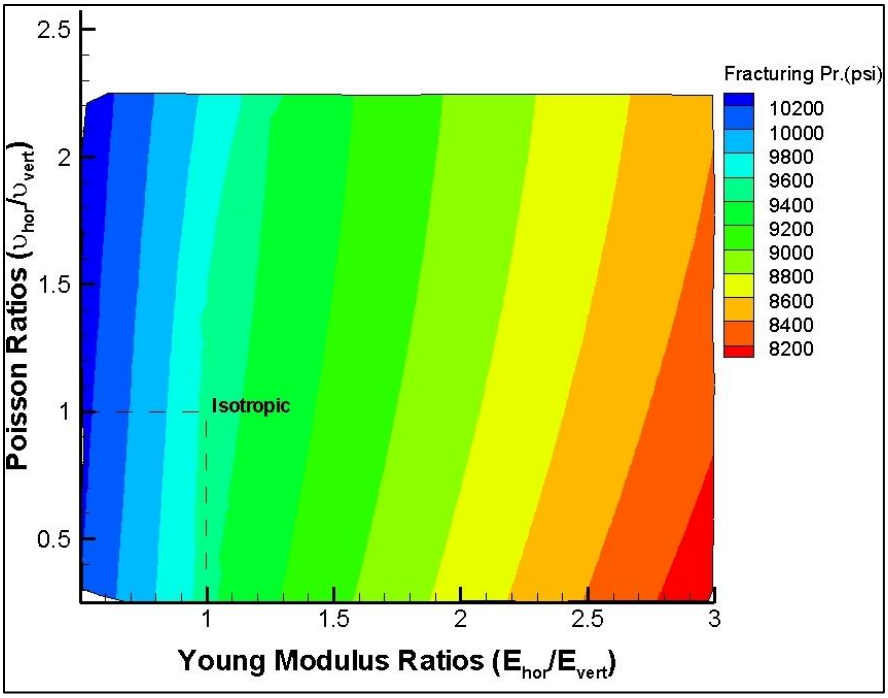

Fig. 12— Fracturing pressure variations in a well drilled along $\sigma_{h\min}$ by changing Young's modulus and Poisson's rations.

There are several points in **Fig. 11** and **Fig. 12** which should be noted:

- The results of the sensitivity analysis clearly show dependency of fracture initiation pressure to variations in $\frac{E_{hor}}{E_{vert}}$ and $\frac{\upsilon_{hor}}{\upsilon_{vert}}$. Depending on the values of Young's modulus and Poisson's ration, the values of fracture initiation pressure may change.
- The case of isotropy is where there is no difference between mechanical properties in different directions. So, in **Fig. 11** and **Fig. 12**, the points of

$\frac{E_{hor}}{E_{vert}} = \frac{\upsilon_{hor}}{\upsilon_{vert}} = 1$ show the pressure required to initiate the tensile fracture (fracture initiation pressure) in the isotropic rock.

- In **Fig. 11** and **Fig. 12**, the contour lines are highly inclined showing that Poisson's ration doesn't significantly contribute in changing the fracture initiation pressure, but at higher Young's modulus ratios, Poisson's ration is also effective in changing the fracturing pressure.
- Unlike the Poisson's ration, the Young's modulus ratio changes the fracturing pressure effectively and significantly. For example, for **Fig. 11**, it can be obviously seen in **Table 4** that when the Poisson's ration is constant at $\frac{\upsilon_{hor}}{\upsilon_{vert}} = 1$, variation of Young's modulus ratio from 0.5 to 1.5 causes about 1151 psi (8877-7726=1151 psi) difference in the value of fracture initiation pressure. However, if the Young's modulus is kept constant at $\frac{E_{hor}}{E_{vert}} = 1$, variations of Poisson's ration from 0.5 to 1.5 can only cause 123 psi (8153-8030=123 psi) difference in the fracturing pressures. **So, the Young's modulus ratio obviously has higher importance in changing the fracture initiation pressure than the Poisson's ration.**
- As can be seen in **Fig. 11** and **Fig. 12**, the contours of fracturing pressure variations are much denser in the case of drilling along $\sigma_{H\max}$ than drilling along

$\sigma_{h\min}$ and it indicates that rock anisotropy has higher effect on changing the fracturing pressure values during drilling along $\sigma_{H\max}$ than along $\sigma_{h\min}$.

- Due to fundamentals of rock mechanics, the materials stiffness has a direct relation with the Young's modulus and an inverse relation with the Poisson's ration. In other words, materials with higher Young's modulus and lower Poisson's ration are respectively stiffer materials (i.e. granite) and those with lower Young's modulus and higher Poisson's ration are softer rocks (i.e. shale).Therefore, since in **Fig. 11** and **Fig. 12**, the lower right corner of the plot has high $\frac{E_{hor}}{E_{vert}}$ and low $\frac{\upsilon_{hor}}{\upsilon_{vert}}$, it represents the case where the rock mass is *stiffer* in horizontal direction. However, the upper left corner in **Fig. 11** and **Fig. 12** corresponds to the case where the vertical direction has higher *stiffness*.
- The results of sensitivity analysis in **Fig. 11** and **Fig. 12** indicate that in normal stress faulting regime where $\sigma_v > \sigma_{H\max} > \sigma_{h\min}$ and drilling along maximum and minimum horizontal stresses, higher stiffness in vertical direction causes more resistance against fracturing and delays the hydraulic fracturing initiation from the well but higher rock mass stiffness in horizontal direction (having respectively lower stiffness in vertical direction) can cause fracturing earlier than the case of isotropic rock.
- The analysis gives a good tool to predict in-situ rock mechanical properties by knowing the fracturing pressure in the field and doing the back analysis. For

example in **Fig. 11** and **Fig. 12**, by assuming $\frac{\upsilon_{hor}}{\upsilon_{vert}}=1$ (for simplicity) and by finding the fracturing pressure from the plot, in-situ $\frac{E_{hor}}{E_{vert}}$ can be estimated.

To better illustrate the importance of the findings, in this study, the fracturing pressure values obtained from those 3000 points in **Fig. 11** are converted to equivalent mud weight at depth of 10,000 ft. (because the well is assumed to be drilled at 10,000 ft. depth).

For example, knowing that the fracturing pressure in **Fig. 11** for isotropic rock is 8000 psi, the mud weight that can cause hydraulic fracture initiation in the isotropic case can be calculated using the equation below:

$$\text{Mw(ppg)}=\frac{\text{Pw(psi)}}{0.052\times\text{D(ft)}}=\frac{8{,}000\text{ psi}}{0.052\times 10{,}000}=15.4\text{ ppg} \quad \text{.....(4.20)}$$

So, it can be said that using 15.38 ppg mud weight in the assumed well can initiate the fracturing around the well.

Fig. 13 shows the equivalent mud weight that can cause fracturing in rock mass when the well is drilled along $\sigma_{H\max}$ with different mechanical properties.

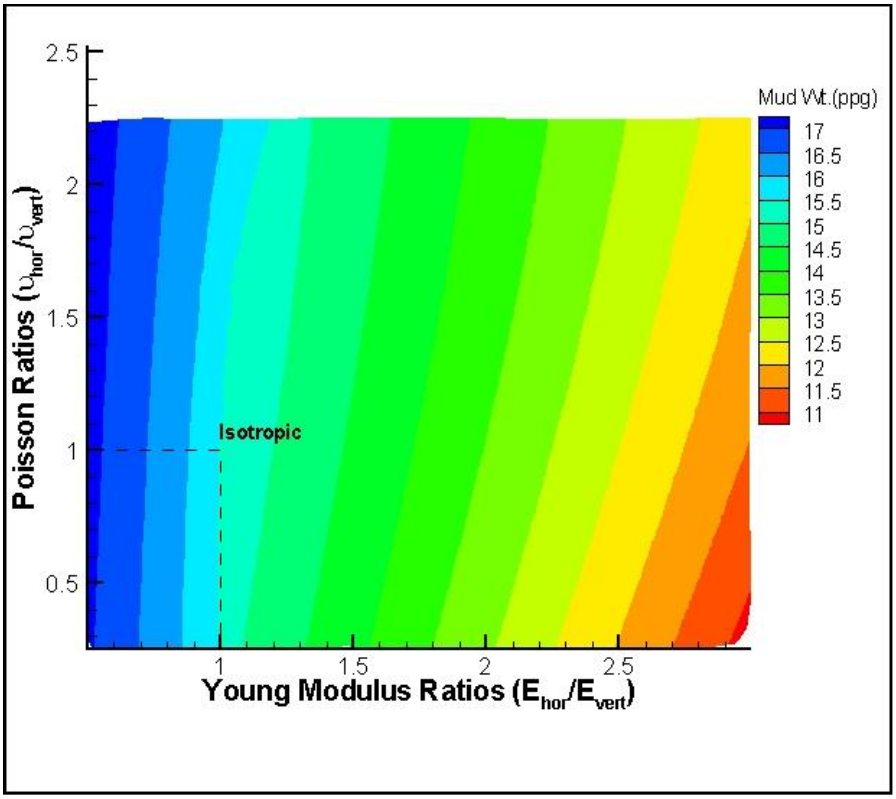

Fig. 13—Variations in equivalent mud weight required to cause fracturing in rocks with different anisotropy ratios.

In **Fig. 13**, it should be noted that:

- The isotropic case with $\frac{E_{hor}}{E_{vert}} = \frac{\upsilon_{hor}}{\upsilon_{vert}} = 1$ shows equivalent mud weight of 15.4 ppg
- As the rock mass stiffness decreases in vertical direction (respective stiffness increases in horizontal direction), which corresponds to lower right corner of **Fig. 13**, the mud weight required to initiate the fracturing decreases. In other words **the rock will break down earlier than expected.** For example, if the required

mud weight to cause fracturing in isotropic rock is ~15.4 ppg, for a rock with $\frac{E_{hor}}{E_{vert}} = 1.5$ and $\frac{\upsilon_{hor}}{\upsilon_{vert}} = 1$, the mud weight falls to 14.85 ppg.

- If rock mass stiffness increases in vertical direction (respective stiffness decreases in horizontal direction), corresponding to upper left corner of **Fig. 13**, the mud weight required to initiate the fracturing increases. In other words **the rock may withstand more pressure without fracturing.** For example, for a rock with $\frac{E_{hor}}{E_{vert}} = 0.5$ (twice higher Young's modulus in vertical direction than horizontal direction) and $\frac{\upsilon_{hor}}{\upsilon_{vert}} = 1$, the fracturing mud weight raises to ~17 ppg.
- So, as an important result, **depending on the respective higher stiffness direction in the transversely isotropic rock, the fracturing pressure and equivalent mud weight can be higher or lower than the fracturing pressure expected with isotropic solutions.** But since in bedded rocks, the rock stiffness is usually higher in horizontal direction, it is expected that the actual fracturing pressure (calculated from anisotropic solutions) is less than the expected value calculated by isotropic solutions.

As another study to show the effects of rock mechanical properties on changing the hydraulic fracture initiation pressure, equation (2.15) and (2.17) were used to calculate shear modulus anisotropy ratio $\frac{G_{hor}}{G_{ver}}$ for the horizontal well drilled along $\sigma_{H\max}$ and using the Young's modulus and Poisson's ration data in **Table 3**.

In this case also, 3000 data points were produced and the fracturing pressure values were calculated for each case and the results are plotted in **Fig. 14**.

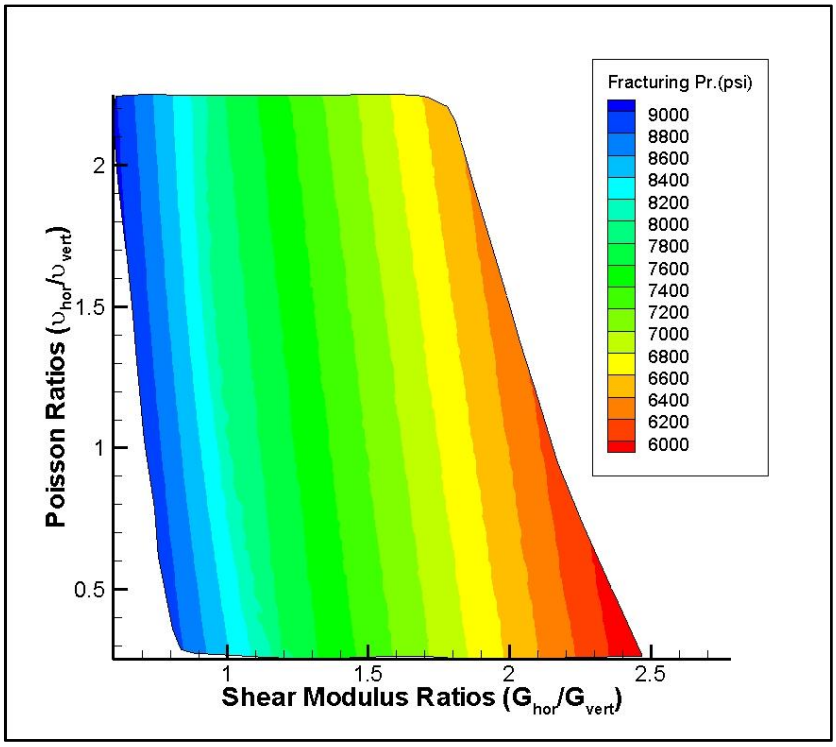

Fig. 14— Fracturing pressure variation by changing shear modulus and Poisson's ration.

As can be seen in the figure above, the same trend between the Young's modulus anisotropy ratio exists for the shear modulus ratio but the effects are less intense. Similar to Young's modulus anisotropy vs. Poisson's ration anisotropy results shown in **Fig. 11**, Poisson's ration has a weak effect on changing the fracture initiation pressure while shear modulus changes the fracturing pressure significantly.

The other important difference is that since the Poisson's ration changes between 0 and 0.5 and due to (2.15), in the isotropic plane, the shear modulus should change between 1/3 to 2/3 of the Young's modulus ratio. So, it can explain the reason why there are no data points for $\frac{G_{hor}}{G_{ver}}$ less than 0.5 and after 2.5.

4.6 Direct and Indirect Estimation of Rock Anisotropy using Experimental Tests

As seen in previous section, estimation of hydraulic fracture initiation pressure is related to an estimate of Young's modulus ratio $\frac{E_{hor}}{E_{vert}}$ and Poisson's ration $\frac{\upsilon_{hor}}{\upsilon_{vert}}$ and the expected fracturing pressure (or equivalent fracturing mud weight) changes by variation in rock anisotropy ratio in shales.

To be able to find the Young's modulus and Poisson's ration anisotropy values we need to use experimental tests to measure Young's modulus and Poisson's ration in 2 orthogonal directions.

In this study, to be able to estimate rock anisotropy, Pierre shale rock was prepared and two sets of core samples were drilled in two different directions:

- Parallel direction to the rock bedding
- Perpendicular direction to the rock bedding

Pierre shale is a geologic formation from upper Cretaceous and expands from North Dakota to New Mexico. It is described as dark gray shale and fossiliferous. The Pierre shale is known for its extremely low permeability but natural fractures improve its

in-situ permeability in some areas and make it commercially attractive for gas production. (Wikipedia 2010)

Fig. 15 shows the coring and rock bedding directions graphically.

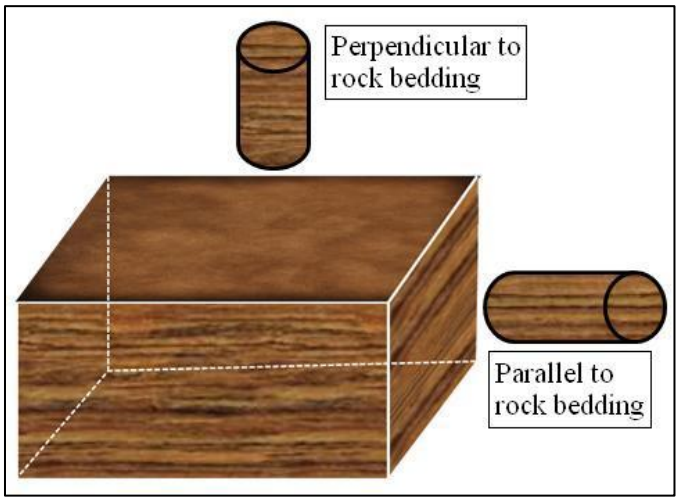

Fig. 15—Respective orientation of rock bedding and the core samples in Pierre shale rock.

The core samples were tested using triaxial testing machine to measure the Young's modulus and Poisson's ration in orthogonal directions directly.

Fig. 16 shows the comparison of Young's modulus for the core sample parallel to the rock bedding with the one being cut in perpendicular direction to the bedding.

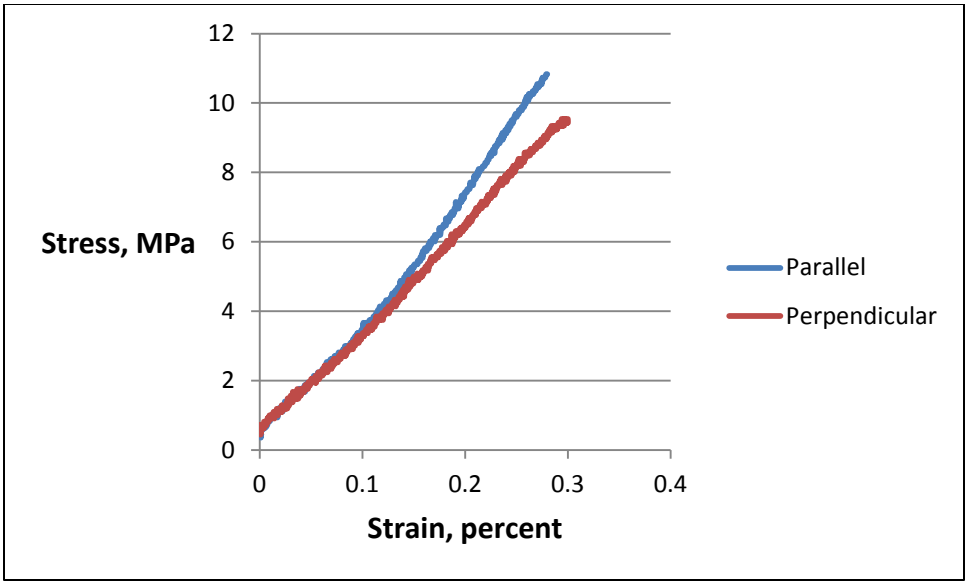

Fig. 16— Comparison of Young's modulus for samples cored in 2 orthogonal directions in Pierre shale rock.

The average Young's modulus for the rock sample in parallel direction was found to be 3.7 GPa (0.53×10^6 psi) and for the perpendicular direction to be 3 GPa (0.43×10^6 psi). So the Young's modulus anisotropy ratio is $\frac{E_{hor}}{E_{vert}} = \frac{3.7}{3} = 1.2$

The Poisson's ration was also measured in two directions and the results were compared as shown in **Fig. 17**.

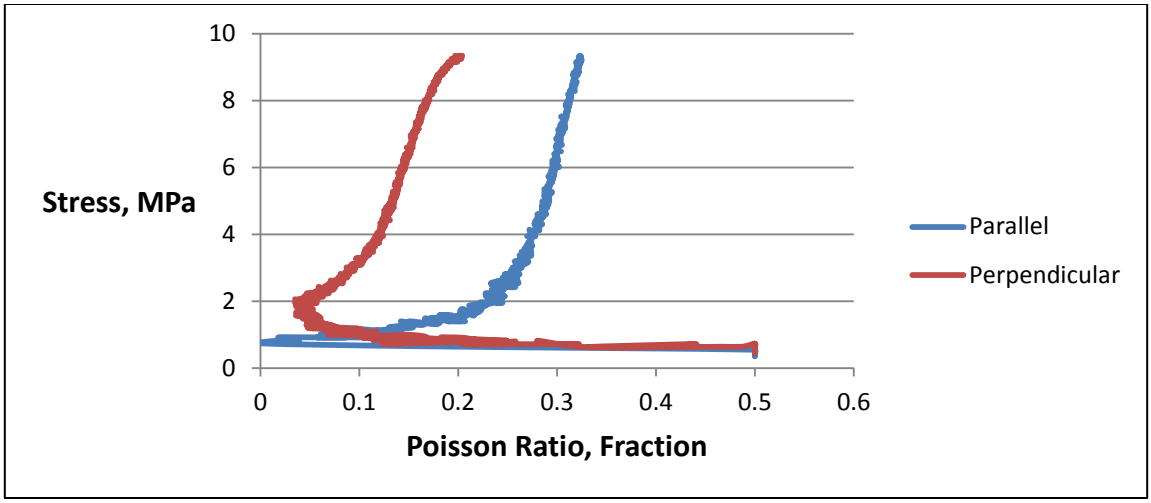

Fig. 17— Comparison of Poisson's ration for samples cored in 2 orthogonal directions in Pierre shale rock.

The Poisson's rations in the linear part were compared to each other and the average Poisson's ration anisotropy was found to be $\frac{\upsilon_{hor}}{\upsilon_{vert}} = \frac{0.28}{0.13} = 2.12$

A short description about the principals of triaxial testing machine is mentioned in Appendix 2.

As another experimental test, we studied the permeability of the two samples mentioned above using pressure pulse permeameter machine .We studied the permeability values in 3 different effective stresses in 2 orthogonal directions and compared the results as shown in **Fig. 18**.

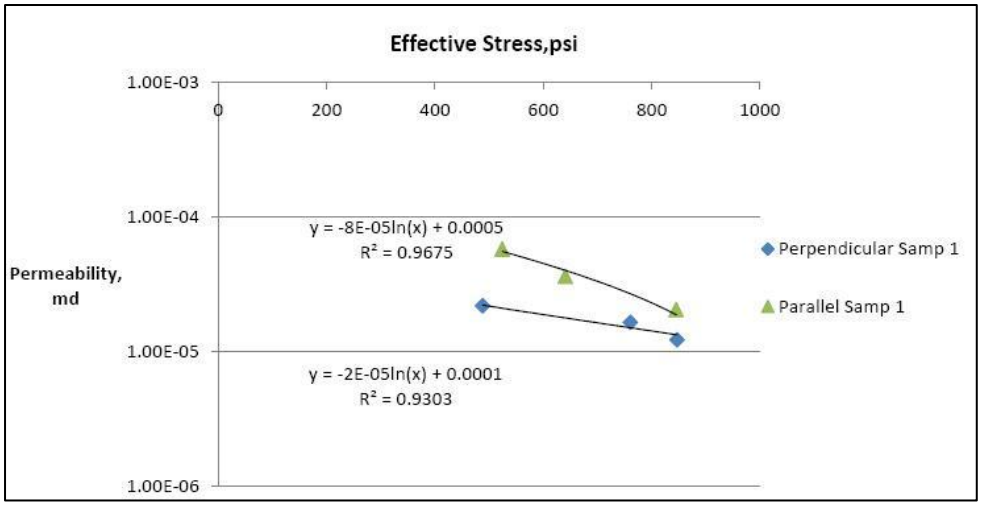

Fig. 18— Stress dependent permeability for Pierre shale samples cored in parallel and perpendicular directions.

The permeability axis has been shown in logarithmic scale as a common method of plotting permeability vs. stress values.

A curve was fitted to each case and a logarithmic function was obtained to each of them. Now using the obtained functions, it is possible to interpolate and estimate the permeability values where the test hasn't been carried out.

Since the effective stress values are not exactly similar in two cases, we need to use interpolation in order to estimate the permeability values in required points. This is done to estimate the anisotropy ratio $(\frac{K_{parallel}}{K_{perpendicular}} = \frac{K_{hor}}{K_{vert}})$ in Pierre shale sample in the range of 450 to 850 psi interval.

To estimate the anisotropy ratio in the range mentioned above, 10 effective stress values are chosen between 450 and 850 psi and divided to each other to find the average permeability anisotropy ratio.

The average permeability anisotropy ratio was found to be $\frac{K_{hor}}{K_{vert}} = 2.18$

4.7 Variations in Fracture Initiation Pressure Caused by Well Orientation and Rock Anisotropy

It is known that, the fracture initiation pressure around the well changes by changing the stress distribution around the well. As mentioned in SECTION 2, the state of stress at any point underground can be shown by 6 components (3 normal and 3 shear stresses) in the stress matrix. The theory of elasticity implies that changing the orientation of the well in respect to in-situ stresses changes the state of stress around the well. Therefore, well orientation is one of the most important factors that play a key role on changing the stress distribution around the well.

There are equations proposed by (Jaeger and Cook 1979) for stress and strain transformation from one state of the stress to another. The problem becomes more complicated for stress and strain transformation calculations in anisotropic rocks since in isotropic rocks the mechanical properties of the rock do not change with orientation. But, in anisotropic (or transversely isotropic) rocks, the effect of anisotropy on the resolution of far-filed stress should also be taken into account. So to get the stress distribution around the well at new orientation in anisotropic rocks, we need to deal with:

- New compliance tensor due to different mechanical properties at different directions
- New stress state due to change in stress conditions

(Amadei 1983) mentioned the transformation matrices that should be used to transfer the compliance tensor from global to the new local orientation system. The transformation matrices are mentioned in Appendix1 of this thesis in detail.

To come up with the effect of formation anisotropy direction and borehole trajectory on the compliance tensor, three different coordination systems are required as shown in **Fig. 19**:

- X,Y,Z is the *global* coordination system which in this study is chosen to coincide with the orientation of in-situ principal stresses
- X', Y', Z' is the coordination system attached to the rectilinear anisotropy. In horizontally laminated rocks, the system X'Y'Z' coincides the global XYZ coordinate system.
- X_b, Y_b, Z_b is the coordination system attached to the borehole (*local* coordination)

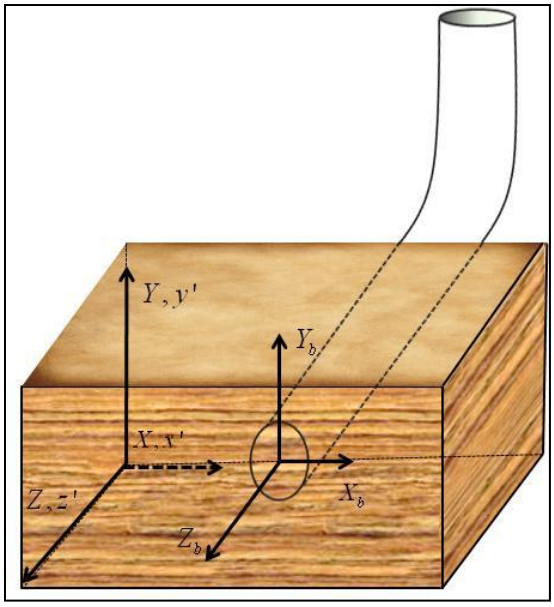

Fig. 19—Three different coordination systems in the anisotropic rocks.

To find the stress compliance tensor in a generic form, the mechanical properties need to be transformed from the anisotropy and borehole coordination systems to a unique system such as the global one. Since in this study, the rock layering is assumed to be horizontal, the rectilinear anisotropy coordinate system coincides with the global one, and simplifies the calculations (**Fig. 19**).The matrix transportation calculations are mentioned in Appendix.1

Fig. 20 shows the orientation of *local* coordination system (attached to the wellbore) in respect to the *global* coordination system which coincides to in-situ stresses. Also **Fig. 21** shows orientation of the plane of rectilinear anisotropy in respect to the *global* coordination system.

Fig. 20 and **Fig. 21** show angles $\delta, \beta, \delta_h, \beta_h$ that should be used in stress and strain transformation analysis (mentioned in Appendix1) to get the final stress state and the final compliance tensor.

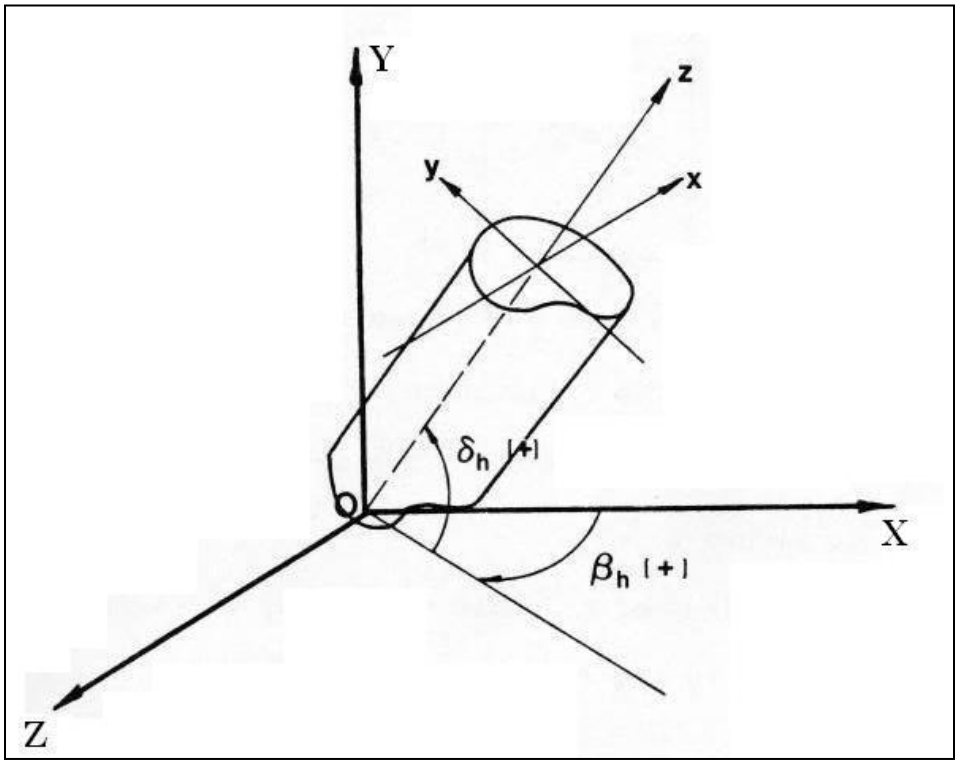

Fig. 20—Orientation of local coordination system vs. the global coordination (principal stresses direction)(Amadei 1983).

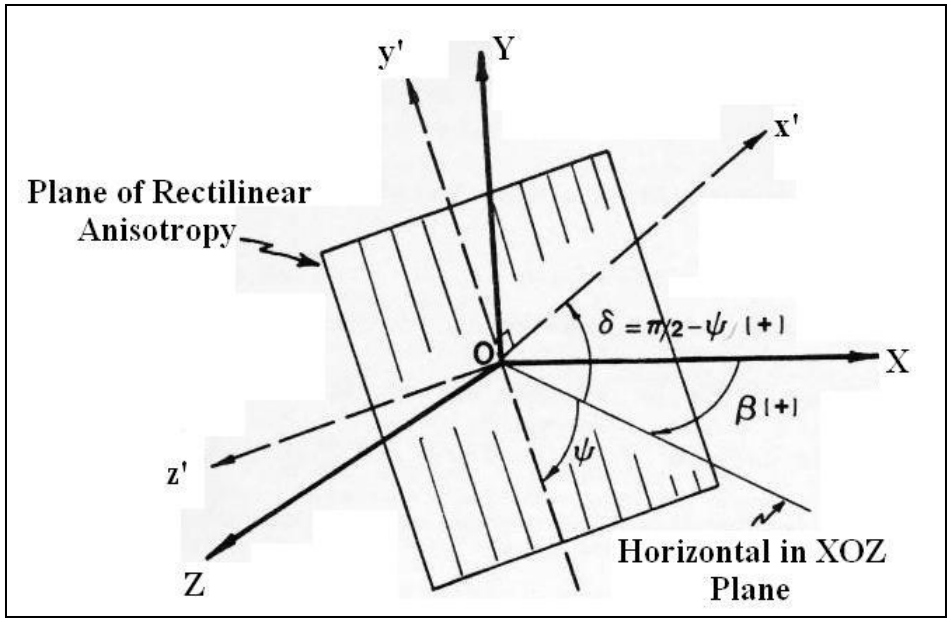

Fig. 21— Orientation of the rectilinear anisotropy plane vs. the global coordination system (principal stresses direction) (Amadei 1983).

Our case is a horizontal well, so in **Fig. 20** the angle $\delta_h = 0°$ to lay the well in horizontal direction in XZ plane and if the goal is to study the variations of fracture initiation pressure when the well orientation varies between maximum horizontal stress $\sigma_{H\max}$ to minimum horizontal stress $\sigma_{h\min}$ direction, the angle β_h should change between 0 and 90 degrees between global Z and X axes. Also since in horizontally layered rock, the plane of rectilinear anisotropy is vertical, angle δ should be 0 degree and angle $\beta = 90°$.

By knowing the angles $\delta, \beta, \delta_h, \beta_h$ and plugging them in equations proposed in Appendix 1 to find the new compliance tensor and state of stress and then using the new analytical solutions described in SECTION 2 and 3, the fracture initiation pressure is calculated for three different anisotropy ratios and variable well orientation.

To carry out the sensitivity analysis, 2 distinct analyses are necessary:

- **Rock Anisotropy**:1 case of isotropy and 2 cases of anisotropy (with $\frac{E_{hor}}{E_{vert}} = 0.8$ and $\frac{E_{hor}}{E_{vert}} = 1.4$) are selected for sensitivity analysis
- **Well orientation**: the orientation of the well changed from maximum horizontal stress $\sigma_{H\max}$ to minimum horizontal stress $\sigma_{h\min}$ direction.

Fig. 22 shows how rock anisotropy and well orientation can change the value of fracture initiation in transversely isotropic rocks.

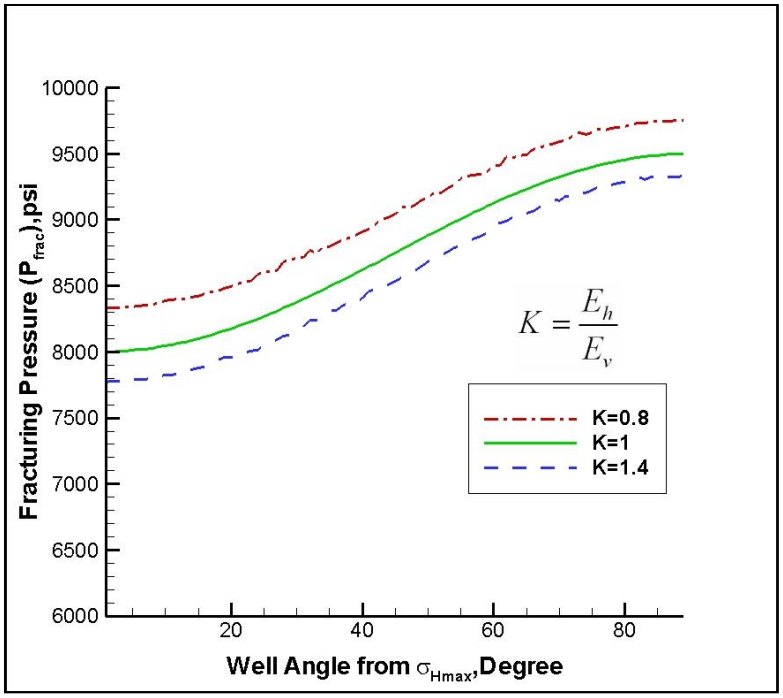

Fig. 22— Fracturing pressure variations caused by well orientation from $\sigma_{H\max}$ and anisotropy ratio $K = \frac{E_{hor}}{E_{vert}}$.

The input parameters of the sensitivity analysis is similar to all other examples and only the variations in Young's modulus ratio $K = \frac{E_{hor}}{E_{vert}}$ and well orientation in respect to $\sigma_{H\max}$ direction was monitored.

Fig. 22 clearly shows that:

- The Young's modulus ratio can change the fracturing pressure even when the well is not drilled along the principal stresses.

- In the case where the Young's modulus ratio is below 1 (for example in **Fig. 22** when $K = \frac{E_{hor}}{E_{vert}} = 0.8$) the fracturing pressure is more than the expected fracturing pressure in isotropic rock. But this pressure is less than the expected fracturing pressure when the Young's modulus ratio is $K = \frac{E_{hor}}{E_{vert}} = 1.4$
- The difference between fracturing pressure in isotropic and anisotropic cases when the wellbore orientation changes stays almost constant. For example the fracturing pressure when $K = \frac{E_{hor}}{E_{vert}} = 1.4$ has about 200 psi difference with $K = \frac{E_{hor}}{E_{vert}} = 1$ and this difference has almost stayed constant when the well trajectory changes.
- As another important result, it is obvious that well trajectory has much bigger effect on changing the fracturing pressure than the anisotropy. For example in this case, the difference in fracturing pressure when well orientation changes from 0 to 90 is over 1,500 psi but the variations caused by rock anisotropy is in the range of 200-300 psi.

Fig. 23 is shown to make **Fig. 22** more understandable.

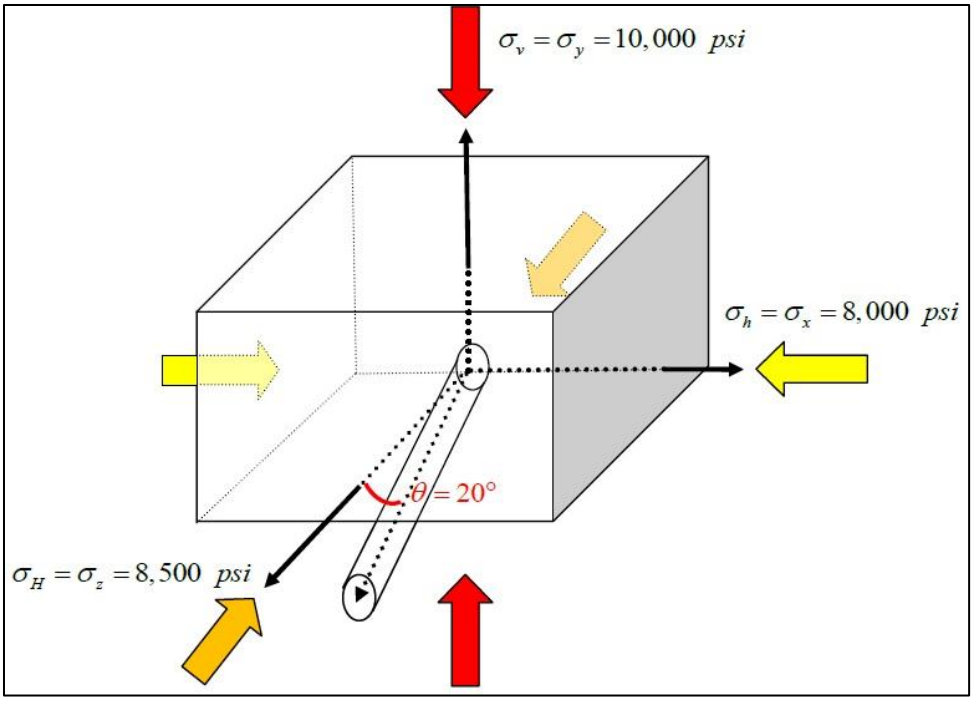

Fig. 23—Variations of horizontal well angle from Z to X axes directions.

As it is shown in **Fig. 23**, the well trajectory changes from the orientation of $\sigma_{H\max}$ to $\sigma_{h\min}$ (From Z to X axis).

In **Fig. 22**, the fracturing pressures associated with the angle of zero show the case where the well is drilled along $\sigma_{H\max}$. The fracturing pressure in this direction, for isotropic and anisotropic rocks can be seen in **Fig. 22**. For example the fracturing pressure for the isotropic rock is 8000 psi as expected but this pressure decreases to ~ 7800 psi when the Young's modulus ratio changes to 1.4.

The fracturing pressures associated with the angle of 90 degrees show the case where the well is drilled along $\sigma_{h\min}$. All the points in between, show the fracturing

pressure variations in the cases where the angle changes from 0 to 90 degrees. For example, **Fig. 23** graphically shows when the well has a 20 degrees horizontal with the maximum horizontal stress. To estimate the hydraulic fracture initiation pressure in the well shown in **Fig. 23** where the well has 20 degrees angle from maximum horizontal stress direction, if we draw a vertical line along 20 degrees point in **Fig. 22** and intersect it with any of the 3 cases (with different Young's modulus anisotropy ratio), the hydraulic fracturing pressure can be estimated.

5. CONCLUSIONS AND SUMMARY

The analytical solution for estimating the fracture initiation pressure while drilling in transverse isotropic rocks has been used to assess the impact of rock elastic anisotropy on the fracturing pressure. A sensitivity study on the effects of rock mechanical properties (Young's modulus and Poisson's ration) on the fracture initiation pressure indicates that depending on the preferred stiffness direction in the rock mass, the fracturing pressure may be higher or lower than the fracturing pressure value estimated by isotropic solutions.

The fracturing pressures in wells drilled along maximum horizontal stress are more sensitive to rock elastic anisotropy than the ones drilled along minimum horizontal stress. The angle of a horizontal well with the principal stresses has a higher impact on changing the fracturing pressure than the rock anisotropy. Also, the rock anisotropy effects remain nearly constant when the orientation of the horizontal well changes from $\sigma_{H\max}$ to $\sigma_{h\min}$ directions.

Since assessing the fracturing pressure requires knowledge of anisotropy ratio in transversely isotropic rocks, triaxial test was carried out on Pierre shale samples which were cored in parallel and perpendicular directions to the rock bedding and Young's modulus and Poisson's ration was measured directly for hydraulic fracturing analysis. To assess possibility of replacing rock permeability ratio instead of Young's modulus ratio in hydraulic fracturing studies, pulse Permeameter machine was used and the rock permeability values were measured in two orthogonal directions.

REFERENCES

Aadnoy, B.S. 1988. Modeling of the Stability of Highly Inclined Boreholes in Anisotropic Rock Formations (Includes Associated Papers 19213 and 19886). *SPE Drilling Engineering* **3** (3). DOI: 10.2118/16526-PA

Aadnoy, B.S. 1989. Stresses around Horizontal Boreholes Drilled in Sedimentary Rocks. *Journal of Petroleum Science and Engineering* **2** (4): 349-360. DOI: 10.1016/0920-4105(89)90009-0

Aadnoy, B.S. and Chenevert, M.E. 1987. Stability of Highly Inclined Boreholes (Includes Associated Papers 18596 and 18736). *SPE Drilling Engineering* **2** (4). DOI: 10.2118/16052-PA

Abousleiman, Y. and Cui, L. 1998. Poroelastic Solutions in Transversely Isotropic Media for Wellbore and Cylinder. *International Journal of Solids and Structures* **35** (34-35): 4905-4929. DOI: DOI: 10.1016/s0020-7683(98)00101-2

Amadei, B. 1983. *Rock Anisotropy and the Theory of Stress Measurements*. Berlin: Springer-Verlag. Original edition. ISBN 0387123881, 9780387123882.

Batugin, S. and Nirenburg, R. 1972. Approximate Relation between the Elastic Constants of Anisotropic Rocks and the Anisotropy Parameters. *Journal of Mining Science* **8** (1): 5-9. DOI: 10.1007/bf02497798

Cauwelaert, F.V. 1977. Coefficients of Deformation of an Anisotropic Body. *Journal of the Engineering Mechanics Division* **103** (5): 823-835.

Daneshy, A.A. 1973. A Study of Inclined Hydraulic Fractures. *Journal of the Society of Petroleum Engineers* **13** (2). DOI: 10.2118/4062-PA

Deily, F.H. and Owens, T.C. 1969. Stress Around a Wellbore. Paper SPE 2557 presented at the Fall Meeting of the Society of Petroleum Engineers of AIME, Denver, Colorado, 28 September-1 October.

Ellefsen, K.J., Toksoz, M.N., Tubman, K.M., and Cheng, C.H. 1992. Estimating a Shear Modulus of a Transversely Isotropic Formation. *Geophysics* **57** (11): 1428-1434. DOI: 10.1190/1.1443210

Goodman, R.E. 1989. *Introduction to Rock Mechanics*. New York/Chichester/Brisbane/Toronto/Singapore. Original edition, John Wiley and Sons Publication. ISBN 0-471-81200-5.

Haimson, B. and Fairhurst, C. 1967. Initiation and Extension of Hydraulic Fractures in Rocks. *Journal of the Society of Petroleum Engineers.* **7** (3): 310 - 318. DOI: 10.2118/1710-PA

Hossain, M.M., Rahman, M.K., and Rahman, S.S. 2000. Hydraulic Fracture Initiation and Propagation: Roles of Wellbore Trajectory, Perforation and Stress Regimes. *Journal of Petroleum Science and Engineering* **27** (3-4): 129-149. DOI: 10.1016/s0920-4105(00)00056-5

Hsiao, C. 1988. A Study of Horizontal-Wellbore Failure. *SPE Production Engineering* **3** (4). DOI: 10.2118/16927-PA

Hubbert, M.K. and Willis, D.G. 1957. Mechanics of Hydraulic Fracturing. *Petr. Trans. AIME* **210**: 153-163.

Jaeger, J.C., Cook, N.G.W., and Zimmerman, R.W. 2007. *Fundamentals of Rock Mechanics,* Fourth Edition. Blackwell Publishing. Original edition. ISBN 978-0-632-05759-.

Jaeger, J.C. and Cook, N.W.G. 1979. *Fundamentals of Rock Mechanics*. New York: Chapman and Hall. Original edition. ISBN: 0632057599, 9780632057597.

Kirsch. 1898. The Theory of Elasticity and the Need of the Strength of Materials(Trans.). *Journal of the Association of German Engineers* **42**: 797-807.

Kwon, O., Kronenberg, A. K., Gangi, A. F., and Johnson, B. 2001. Permeability of Wilcox Shale and Its Effective Pressure Law. *Journal of Geophysical Research* **106** (B9): 19339-19353.

Lekhnitskii, S.G. 1963. *Theory of Elasticity of an Anisotropic Elastic Body*. San Fransisco: Holden Day Inc. Original edition.

Lekhnitskii, S.G. 1981. *Theory of Elasticity of an Anisotropic Body*. Moscow: Mir Publications. Original edition.

Ning, X. 1992. The Measurement of Matrix and Fracture Properties in Naturally Fractured Low Permeability Cores Using a Pressure Pulse Method. Ph.D. Dissertation, Texas A&M University.

Ong, S.H. 1994. Borehole Stability. Ph.D. Dissertation, The University of Oklahoma.

Ong, S.H. and Roegiers, J.-C. 1993. Horizontal Wellbore Collapse in an Anisotropic Formation. Paper SPE 25504 presented at the SPE Production Operations Symposium, Oklahoma City, Oklahoma, 21-23 March.

Ong, S.H. and Roegiers, J.-C. 1996. Fracture Initiation from Inclined Wellbores in Anisotropic Formations. *SPE Journal of Petroleum Technology* **48** (7). DOI: 10.2118/29993-PA

Suarez-Rivera, R., Green, S.J., McLennan, J., and Bai M. 2006. Effect of Layered Heterogeneity on Fracture Initiation in Tight Gas Shales. Paper SPE 103327 presented at the SPE Annual Technical Conference and Exhibition, San Antonio, Texas, 24-27 September.

Wikipedia, 2010. Pierre Shale. http://en.wikipedia.org/wiki/Pierre_Shale.

APPENDIX 1

STRESS AND STRAIN TRANSFORMATION CALCULATIONS

If we define the stress and strain components in matrix form for *global* coordination as below:

$$(\sigma)^t_{XYZ} = \begin{pmatrix} \sigma_X & \sigma_Y & \sigma_Z & \tau_{YZ} & \tau_{XZ} & \tau_{XY} \end{pmatrix} \quad \text{(A.1)}$$

$$(\varepsilon)^t_{XYZ} = (\varepsilon_X \quad \varepsilon_Y \quad \varepsilon_Z \quad \gamma_{YZ} \quad \gamma_{XZ} \quad \gamma_{XY}) \quad \text{(A.2)}$$

And in rectilinear anisotropy coordination as:

$$(\sigma)^t_{X'Y'Z'} = \begin{pmatrix} \sigma_{X'} & \sigma_{Y'} & \sigma_{Z'} & \tau_{Y'Z'} & \tau_{X'Z'} & \tau_{X'Y'} \end{pmatrix} \quad \text{(A.3)}$$

$$(\varepsilon)^t_{X'Y'Z'} = (\varepsilon_{X'} \quad \varepsilon_{Y'} \quad \varepsilon_{Z'} \quad \gamma_{Y'Z'} \quad \gamma_{X'Z'} \quad \gamma_{X'Y'}) \quad \text{(A.4)}$$

And in borehole direction as:

$$(\sigma)^t_{X_bY_bZ_b} = \begin{pmatrix} \sigma_{X_b} & \sigma_{Y_b} & \sigma_{Z_b} & \tau_{Y_bZ_b} & \tau_{X_bZ_b} & \tau_{X_bY_b} \end{pmatrix} \quad \text{(A.5)}$$

$$(\varepsilon)^t_{X_bY_bZ_b} = (\varepsilon_{X_b} \quad \varepsilon_{Y_b} \quad \varepsilon_{Z_b} \quad \gamma_{Y_bZ_b} \quad \gamma_{X_bZ_b} \quad \gamma_{X_bY_b}) \quad \text{(A.6)}$$

So the purpose is to find the constitutive equation in a case of a well which might not be drilled along the principal stresses and the plane of anisotropy in the field.

The constitutive equation in anisotropic coordination of X'Y'Z' is as follows:

$$(\varepsilon)_{X'Y'Z'} = (H').(\sigma)_{X'Y'Z'} \quad \text{(A.7)}$$

where:

H' is the new compliance tensor in anisotropic coordination system

The relation between the stresses in the global system and the anisotropic coordination system is as below:

$$(\sigma)_{X'Y'Z'} = (T_\sigma)_{X'Y'Z'}.(\sigma)_{XYZ} \quad \text{(A.8)}$$

In fact, $(T_\sigma)_{X'Y'Z'}$ is the transformation matrix which is multiplied to the global stresses matrix to result the stresses in the rectilinear anisotropic coordination and will be illustrated later on SECTION A.1.2.

The same type of relation governs between strain in the global and rectilinear anisotropy coordination systems, where:

$$(\varepsilon)_{X'Y'Z'} = (T_\varepsilon)_{X'Y'Z'}.(\varepsilon)_{XYZ} \quad \text{(A.9)}$$

where $(T_\varepsilon)_{X'Y'Z'}$ is the transformation matrix which transforms the strains from global to rectilinear anisotropy coordination system.

In the transformation matrices, there is a relation between $(T_\varepsilon)_{X'Y'Z'}$ and $(T_\sigma)_{X'Y'Z'}$:

$$(T_\varepsilon)^{-1}_{X'Y'Z'} = (T_\sigma)^{t}_{X'Y'Z'} \quad \text{(A.10)}$$

$$(T_\varepsilon)^{t}_{X'Y'Z'} = (T_\sigma)^{-1}_{X'Y'Z'} \quad \text{(A.11)}$$

where the superscripts “-1” and “t” denotes inverse and transpose matrices respectively.

If we substitute (A.8) and (A.9) into (A.7) and use (A.10) and (A.11) , the constitutive equation in the global coordination system can be calculated using:

$$(\varepsilon)_{XYZ} = (T_\sigma)^{t}_{X'Y'Z'}.H'.(T_\sigma)_{X'Y'Z'}.(\sigma)_{XYZ} \quad \text{(A.12)}$$

The new constitutive equation results from multiplication of $(T_\sigma)^{t}_{X'Y'Z'}$, H’ and $(T_\sigma)_{X'Y'Z'}$ matrices. Using the equation above, the constitutive equation in the global coordination system can be calculated by knowing the transformation matrix (which will be illustrated later) and the constitutive matrix in rectilinear anisotropy coordination.

In the second case, If the wellbore has a different coordination from the global system or in other words, if the well is not drilled along the principal stresses, then the constitute equations for the rock mass around the wellbore are definitely different from the global constitutive equations.

The transformation equation between the global and local (attached to the wellbore) systems are as below:

$$(\sigma)_{X_bY_bZ_b} = (T_\sigma)_{X_bY_bZ_b}.(\sigma)_{XYZ} \quad \text{(A.13)}$$

$$(\varepsilon)_{X_bY_bZ_b} = (T_\varepsilon)_{X_bY_bZ_b}.(\varepsilon)_{XYZ} \quad \text{(A.14)}$$

where $(T_\sigma)_{X_bY_bZ_b}$ and $(T_\varepsilon)_{X_bY_bZ_b}$ are the matrices which transform the stress and strain components in global coordination system (in-situ principal stresses) to the local system (attached to the wellbore) and will be illustrated in SECTION A.1.2 of this appendix.

In the transformation matrices, there is a relation between $(T_\varepsilon)_{X_bY_bZ_b}$ and $(T_\sigma)_{X_bY_bZ_b}$:

$$(T_\varepsilon)^{-1}_{X_bY_bZ_b} = (T_\sigma)^{t}_{X_bY_bZ_b} \quad \text{(A.15)}$$

$$(T_\varepsilon)^{t}_{X_bY_bZ_b} = (T_\sigma)^{-1}_{X_bY_bZ_b} \quad \text{(A.16)}$$

By substitution of (A.13) and (A.14) into (A.12) to find out the simultaneous effect of different wellbore direction and plane of anisotropy and by using (A.15) and (A.16), equation below is obtained for the constitutive relation in local coordination system for a well drilled with arbitrary trajectory and plane of anisotropy orientations .

$$(\varepsilon)_{X_bY_bZ_b} = (T_\varepsilon)_{X_bY_bZ_b}.(T_\sigma)^{t}{}_{X'Y'Z'}.H'.(T_\sigma)_{X'Y'Z'}.(T_\varepsilon)^{t}_{X_bY_bZ_b}.(\sigma)_{X_bY_bZ_b} \quad \text{(A.17)}$$

And if we assume A as the new compliance matrix, since we should have:

$$(\varepsilon)_{X_bY_bZ_b} = A.(\sigma)_{X_bY_bZ_b} \quad \text{(A.18)}$$

Therefore, the final compliance matrix is:

$$A = (T_\varepsilon)_{X_bY_bZ_b}.(T_\sigma)^t_{X'Y'Z'}.H'.(T_\sigma)_{X'Y'Z'}.(T_\varepsilon)^t_{X_bY_bZ_b} \quad \text{(A.19)}$$

The equation above states that to calculate the compliance tensor and the constitutive equation in local wellbore coordination system in presence of different anisotropy and principal stress orientations, we need to have the compliance tensor in rectilinear anisotropy coordination (Matrix H') and multiply it to the stress and strain transformation matrices. In sections below, these transformation matrices are illustrated more in detail

A.1 Transformation of Elastic Constants

A.1.1 Compliance Tensor Transformation Caused by Anisotropy

Fig. 24 shows the orientation of the coordination system XYZ and X'Y'Z' in anisotropic rock.

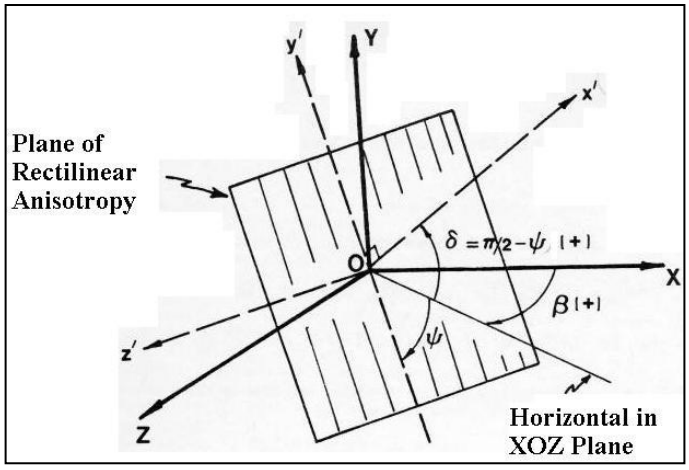

Fig. 24—Orientation of global coordination system vs. the coordination system attached to the plane of rectilinear anisotropy (Amadei 1983).

(Amadei 1983) proposed a transformation matrix which by knowing the constitutive relation of an anisotropic material in the X, Y', Z' coordination system and the angles δ, β as shown in **Fig. 24**, the constitutive equations in the global coordination system can be obtained.

The direction cosines of the transformation matrix from X'Y'Z' to XYZ coordination systems are defined as follows:

$$\begin{bmatrix} l_{X'} = \cos(X, X') & l_{Y'} = \cos(X, Y') & l_{Z'} = \cos(X, Z') \\ m_{X'} = \cos(Y, X') & m_{Y'} = \cos(Y, Y') & m_{Z'} = \cos(Y, Z') \\ n_{X'} = \cos(Z, X') & n_{Y'} = \cos(Z, Y') & n_{Z'} = \cos(Z, Z') \end{bmatrix} \quad \text{..... (A.20)}$$

To calculate these direction cosines in respect to angles δ, β, (Amadei 1983) proposed the equations below:

$$\begin{bmatrix} l_{X'} = \cos\delta_{X'}.\cos\beta_{X'} & l_{Y'} = \cos\delta_{Y'}.\cos\beta_{Y'} & l_{Z'} = \cos\delta_{Z'}.\cos\beta_{Z'} \\ m_{X'} = \sin\delta_{X'} & m_{Y'} = \sin\delta_{Y'} & m_{Z'} = \sin\delta_{Z'} \\ n_{X'} = \cos\delta_{X'}.\sin\beta_{X'} & n_{Y'} = \cos\delta_{Y'}.\sin\beta_{Y'} & n_{Z'} = \cos\delta_{Z'}.\sin\beta_{Z'} \end{bmatrix} \quad \text{..... (A.21)}$$

where:

$$\beta_{X'} = \beta \quad \beta_{Y'} = \beta + \pi \quad \beta_{Z'} = \beta + \frac{\pi}{2}$$

$$\delta_{X'} = \delta \quad \delta_{Y'} = \frac{\pi}{2} - \delta \quad \delta_{Z'} = 0$$

Since in this study, the main objective is to assess the hydraulic fracturing initiation in horizontal wells embedded inside horizontal transverse isotropic rocks, the global and anisotropic coordination axes should coincide. By choosing $\alpha, \beta = 0°$ in **Fig. 24** the direction cosines in (A.21) will change to:

$$\begin{bmatrix} l_{X'} = \cos 0°.\cos 0° = 1 & l_{Y'} = \cos(\frac{\pi}{2}).\cos(\pi) = 0 & l_{Z'} = \cos 0°.\cos\frac{\pi}{2} = 0 \\ m_{X'} = \sin 0° = 0 & m_{Y'} = \sin(\frac{\pi}{2}) = 1 & m_{Z'} = \sin 0 = 0 \\ n_{X'} = \cos 0°.\sin 0° = 0 & n_{Y'} = \cos(\frac{\pi}{2}).\sin(\pi) = 0 & n_{Z'} = \cos 0.\sin(\frac{\pi}{2}) = 1 \end{bmatrix} \quad \text{..... (A.22)}$$

The matrix above becomes an identity matrix with diagonal values equal to 1 which in fact has no effect on the transformation matrix. But if we choose other values of α, β - meaning the well has an acute angle with the plane of isotropy- then the results might be different. (Goodman 1989) suggested the matrix below for stress transformation matrix $(T_\sigma)_{X'Y'Z'}$

$$(T_\sigma)_{X'Y'Z'} = \begin{bmatrix} l_{X'}^2 & m_{X'}^2 & n_{X'}^2 & 2m_{X'}n_{X'} & 2n_{X'}l_{X'} & 2l_{X'}m_{X'} \\ l_{Y'}^2 & m_{Y'}^2 & n_{Y'}^2 & 2m_{Y'}n_{Y'} & 2n_{Y'}l_{Y'} & 2l_{Y'}m_{Y'} \\ l_{Z'}^2 & m_{Z'}^2 & n_{Z'}^2 & 2m_{Z'}n_{Z'} & 2n_{Z'}l_{Z'} & 2l_{Z'}m_{Z'} \\ l_{Y'}.l_{Z'} & m_{Y'}.m_{Z'} & n_{Y'}.n_{Z'} & m_{Y'}.n_{Z'} + n_{Y'}.m_{Z'} & n_{Y'}l_{Z'} + n_{Z'}l_{Y'} & l_{Y'}m_{Z'} + l_{Z'}m_{Y'} \\ l_{Z'}.l_{X'} & m_{Z'}.m_{X'} & n_{Z'}.n_{X'} & m_{Z'}.n_{X'} + n_{Z'}.m_{X'} & n_{X'}l_{Z'} + n_{Z'}l_{X'} & l_{X'}m_{Z'} + l_{Z'}m_{X'} \\ l_{X'}.l_{Y'} & m_{X'}.m_{Y'} & n_{X'}.n_{Y'} & m_{X'}.n_{Y'} + n_{X'}.m_{Y'} & n_{X'}l_{Y'} + n_{Y'}l_{X'} & l_{X'}m_{Y'} + l_{Y'}m_{X'} \end{bmatrix} \quad \text{... (A.23)}$$

If the global and the anisotropy coordination systems coincide, which can happen in the case of a horizontally deposited reservoir with horizontal and vertical principal in-situ stresses, by replacing the components of the transformation matrix calculated in (A.22) in (A.23) , the transformation matrix for anisotropy $(T_\sigma)_{X'Y'Z'}$ changes to:

$$(T_\sigma)_{X'Y'Z'} = \begin{bmatrix} 1 & 0 & 0 & 0 & 0 & 0 \\ 0 & 1 & 0 & 0 & 0 & 0 \\ 0 & 0 & 1 & 0 & 0 & 0 \\ 0 & 0 & 0 & 1 & 0 & 0 \\ 0 & 0 & 0 & 0 & 1 & 0 \\ 0 & 0 & 0 & 0 & 0 & 1 \end{bmatrix} \quad \text{..... (A.24)}$$

The matrix of (A.24) should be replaced in final compliance tensor matrix calculations in equation (A.19)

A.1.2 Compliance Tensor Transformation Caused by Well Orientation

Fig. 25 shows the orientation of the global coordination system XYZ vs. local system $X_bY_bZ_b$.

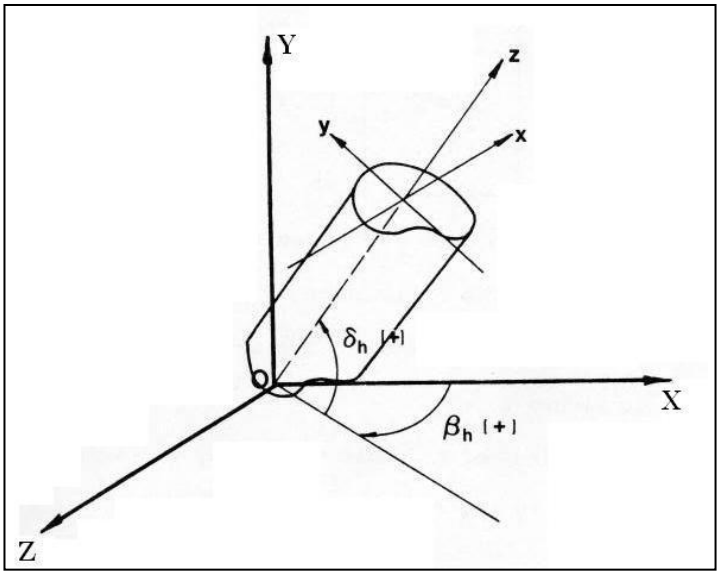

Fig. 25— Orientation of global vs. local coordinate systems.

The direction cosines should be calculated as follows:

$$\begin{bmatrix} l_{X_b} = \cos\delta_X \,.\cos\beta_{X_b} & l_{Y_b} = \cos\delta_Y .\cos\beta_{Y'} & l_{Z_b} = \cos\delta_Z .\cos\beta_Z \\ m_{X_b} = \sin\delta_X & m_{Y_b} = \sin\delta_Y & m_{Z_b} = \sin\delta_Z \\ n_{X_b} = \cos\delta_X .\sin\beta_X & n_{Y_b} = \cos\delta_Y .\sin\beta_Y & n_{Z_b} = \cos\delta_Z .\sin\beta_Z \end{bmatrix} \quad \text{..... (A.25)}$$

where:

$$\begin{matrix} \beta_{X_b} = \beta_h + \dfrac{3\pi}{2} & \beta_{Y_b} = \beta_h + \pi & \beta_{Z_b} = \beta_h \\ \delta_{X_b} = 0 & \delta_{Y_b} = \dfrac{\pi}{2} - \delta_h & \delta_{Z'} = \delta_h \end{matrix} \quad \text{..... (A.26)}$$

Since in this study, the goal is to assess horizontal wells, the angle β_h should be 90 degrees to lay the well orientation horizontally, but the angle δ_h can vary between 0 and 90 degrees. So the direction cosines will change to:

$$\begin{bmatrix} l_{X_b}=\cos 0°.\cos 2\pi=1 & l_{Y_b}=\cos(\frac{\pi}{2}-\delta_h).\cos(\frac{3\pi}{2})=0 & l_{Z_b}=\cos\delta_h.\cos\frac{\pi}{2}=0 \\ m_{X_b}=\sin 0°=0 & m_{Y_b}=\sin(\frac{\pi}{2}-\delta_h) & m_{Z_b}=\sin\delta_h \\ n_{X_b}=\cos 0°.\sin 2\pi=0 & n_{Y_b}=-\cos(\frac{\pi}{2}-\delta_h) & n_{Z_b}=\cos\delta_h \end{bmatrix} \quad \text{..... (A.27)}$$

The stress transformation matrix for the borehole coordination system is the same as the transformation matrix used for anisotropy coordination. What we need is simply replacing the direction cosines used in (A.23) with the ones calculated in (A.27).

To calculated Strain compliance tensor $(T_\varepsilon)_{X_bY_bZ_b}$, the same direction cosines calculated in (A.27) are plugged in equation below to obtain the strain transformation matrix:

$$(T_\varepsilon)_{X_bY_bZ_b}=\begin{bmatrix} l_{X_b}^2 & m_{X_b}^2 & n_{X_b}^2 & m_{X_b}n_{X_b} & n_{X_b}l_{X_b} & l_{X_b}m_{X_b} \\ l_{Y_b}^2 & m_{Y_b}^2 & n_{Y_b}^2 & m_{Y_b}n_{Y_b} & n_{Y_b}l_{Y_b} & l_{Y_b}m_{Y_b} \\ l_{Z_b}^2 & m_{Z_b}^2 & n_{Z_b}^2 & m_{Z_b}n_{Z_b} & n_{Z_b}l_{Z_b} & l_{Z_b}m_{Z_b} \\ 2l_{Y_b}.l_{Z_b} & 2m_{Y_b}.m_{Z_b} & 2n_{Y_b}.n_{Z_b} & m_{Y_b}.n_{Z_b}+n_{Y_b}.m_{Z_b} & n_{Y_b}l_{Z_b}+n_{Z_b}l_{Y_b} & l_{Y_b}m_{Z_b}+l_{Z_b}m_{Y_b} \\ 2l_{Z_b}.l_{X_b} & 2m_{Z_b}.m_{X_b} & 2n_{Z_b}.n_{X_b} & m_{Z_b}.n_{X_b}+n_{Z_b}.m_{X_b} & n_{X_b}l_{Z_b}+n_{Z_b}l_{X_b} & l_{X'}m_{Z'}+l_{Z_b}m_{X_b} \\ 2l_{X_b}.l_{Y_b} & 2m_{X'}.m_{Y'} & 2n_{X_b}.n_{Y_b} & m_{X_b}.n_{Y_b}+n_{X_b}.m_{Y_b} & n_{X_b}l_{Y_b}+n_{Y_b}l_{X_b} & l_{X_b}m_{Y_b}+l_{Y_b}m_{X_b} \end{bmatrix} \quad \text{... (A.28)}$$

The matrix of (A.28) should be replaced in final compliance tensor matrix calculations (A.19).

APPENDIX 2
EXPERIMENTAL METHODS TO MEASURE ROCK ANISOTROPY IN SHALES

In previous sections, analytical methods are used and developed to estimate the fracturing initiation pressure in transversely isotropic rocks. As seen, fracturing pressure is in direct relation with rock mechanical properties such as Young's modulus and Poisson's ration. In anisotropic and transversely isotropic rocks, due to the intrinsic variations of mechanical properties in different direction of the rock mass, estimation or measuring such properties is not easy. Routine log analysis methods can only estimate the mechanical properties indirectly and in a single direction and usually cannot predict the rock behavior in the direction perpendicular to the well. Therefore, it is essential to use core analysis methods to measure (and not estimate) the rock mechanical properties to use them in the equations.

From the engineering point of view, core analysis is the use of the core samples obtained from the drilling operation to obtain the properties of the rock in the reservoir. A good analysis of the core samples can give us valuable information about the behavior of the reservoir rock and eventually lead to proper formation evaluation, drilling method selection and production estimation. Core analysis is usually subdivided to "Routine" and "Special" Core Analysis. Routine Core Analysis is a set of measurements that can be made with minimal preservation. Porosity, grain density, fluid and/or gas saturation and absolute permeability are among the most important "Routine Core Analysis". Any other measurement that can be made on the core samples and are not categorized as a "Routine Core Analysis" should be discussed in "Special Core Analysis".

In this appendix, 2 special core analysis methods will be used to *measure directly* and *estimate indirectly* the rock anisotropy in transversely isotropic rocks.

In this study, rock anisotropy will be measured and estimated in two different ways:

1. **Directly:** Triaxial testing machine will be used to measure the Young's modulus and Poisson's rations directly
2. **Indirectly:** Rock permeability anisotropy ($\frac{K_{hor}}{K_{vert}}$) will be measured using pressure pulse permeameter machine and will be compared with Young's modulus ratio to see if it can be used as a substitute to the direct measurement methods.

As the first way of measuring rock anisotropy, in the next section triaxial testing method will be explained and discussed briefly.

Also in SECTION 5.3, pressure pulse permeameter method as an indirect method of evaluating the rock anisotropy will be assessed.

A.1 Direct Rock Anisotropy Measurement using Triaxial Testing Machine

Triaxial testing machine enables us to apply axial and confining pressures to the core samples and study variation of the ultimate strength and rock stiffness with variation in confining pressure. Using this machine and by having at least 2 core samples being cut in perpendicular direction in respect to each other, the Young's modulus and also Poisson's ration anisotropy can be measured.

A.2 Indirect Rock Anisotropy Measurement using Pressure Pulse Permeameter Method

As an indirect method of evaluating the rock anisotropy in shales, in this section we focused on "pressure pulse permeability" method and will study the indirect relation between Young's modulus ratio $\frac{E_{hor}}{E_{vert}}$ which is already known in different stress values (from triaxial test) and the permeability anisotropy ratio $\frac{K_{hor}}{K_{vert}}$ in known stress values. The goal of the indirect rock anisotropy studies is to see if permeability anisotropy $\frac{K_{hor}}{K_{vert}}$ can be substituted with Young's modulus anisotropy $\frac{E_{hor}}{E_{vert}}$ in the analyses or if there is a relation between these two between the above mentioned ratios so that by knowing the permeability anisotropy ratio, hydraulic fracture initiation pressure can be estimated.

Different methods are available for permeability measurement in rock samples but "steady state" and "unsteady state" methods are the most common ones. To measure the permeability of tight rock samples such as shales, unsteady state method is more common since the required time for permeability measurement in steady state method for tight samples may reach weeks or months.

A.2.1 System Overview

Pressure Pulse Permeameter is laboratory equipment based on unsteady state measurement and is used in our studies. It has been developed and constructed by (Ning

1992) to conduct pressure pulse tests on fractured core samples but it can also be used in un-fractured samples as well.

It can determine the following parameters, separately in a fractured core sample:

- Porosity of the rock matrix
- Permeability of the rock matrix
- Effective width of the fractures
- Permeability of the fracture

Also, studying the mentioned parameters in various confining pressures (overburden pressure) and reservoir temperature is possible. It measures the matrix properties as low as 10^{-9} md which makes it unique in comparison to other permeability measurement techniques such as steady state method. This capability enables the machine to measure petrophysical parameters of tight (fractured) shale samples precisely and more importantly in a much shorter time.

Fig. 26 shows the schematics of pulse permeability machine.

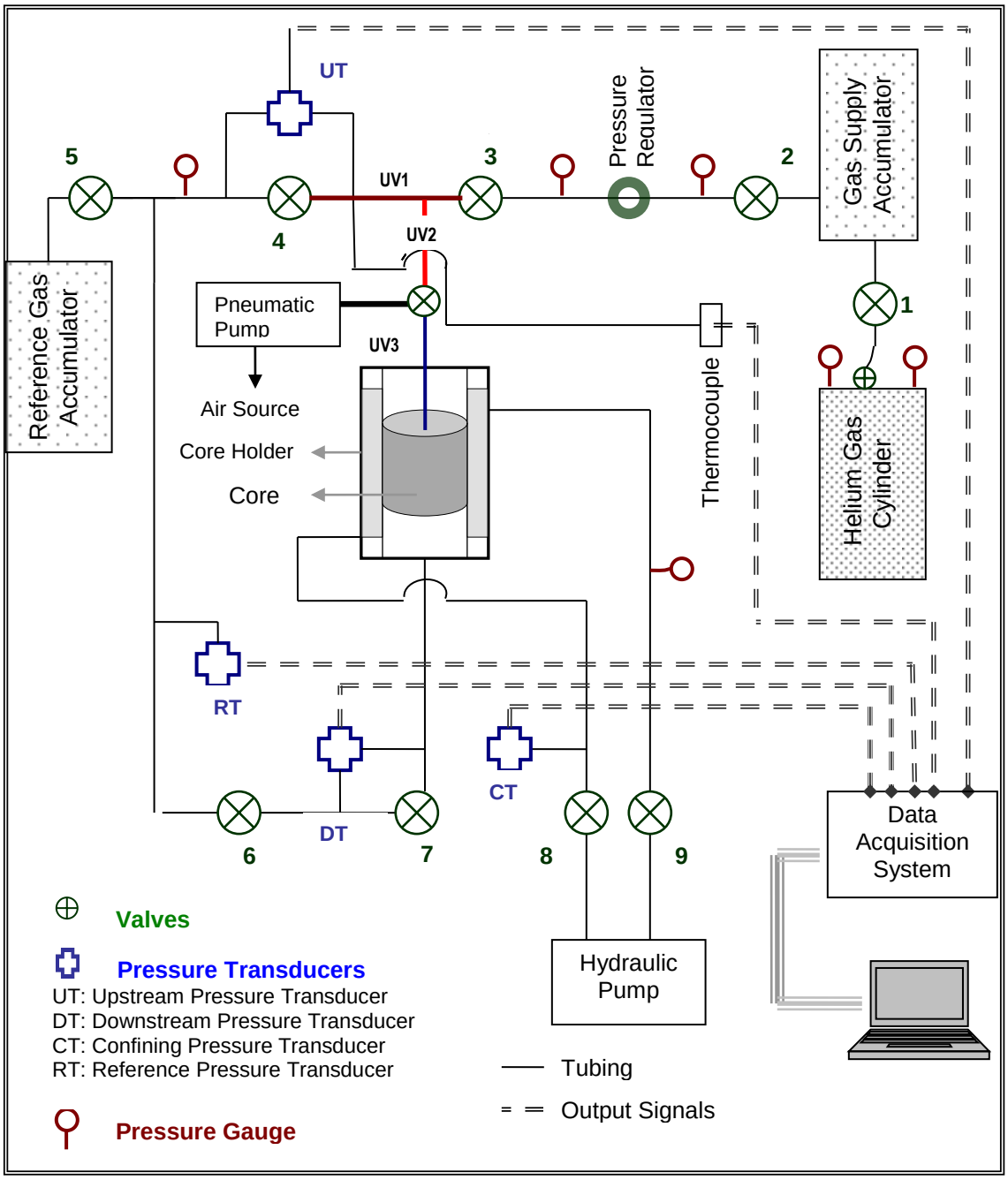

Fig. 26—Schematic of pressure pulse permeameter.

To carry out the test, the core sample is loaded to the machine and saturated with a system (pore) pressure. A desired confining pressure may be applied to the core sample. Then an upstream differential pressure is injected to the core sample. Depending on how permeable/porous the core sample is, the upstream pressure decreases and the downstream pressure increases with time which is acquired and recorded by the data acquisition system. The recorded pressure drawdown values are then reduced and prepared to be used in the history matching program. The last program, using analytical calculations and mathematical history matching suggests the permeability and porosity for the core sample.

A.2.2 Accomplishments on Pulse Permeameter Machine

The pulse permeameter machine had several operational problems and it was necessary to solve them prior to running the tests. Some of the problems and the procedure to solve them are listed below:

- **Calibration and setting up the machine**:

  As mentioned above, since the machine was not operational for a while, the sensitive transducers were out of calibration. Also many connections and fittings were out of used and it was necessary to replace them. Calibration of transducers required very high degree of accuracy and was carried out with great precision. Also setting up the fittings and connections are very sensitive to the amount of torque and force applied to them since over tightening the connections

would damage the fitting threads easily and that was enough to cause the leakage in the system.

- **Leakage**:

Pulse permeameter machine works based on injection of a gas pulse to a core sample which should also be saturated with the gas prior to the test. The core sample is usually saturated with 500-1000 psi gas pressure. So such a high gas pressure increases the chance of the gas leakage from the connections. Since this machine is supposed to measure the permeabilities in nano Darcy scales, any leakage above 0.5-1 psi/hr in the system is not acceptable. Dealing with such a low leakage rate and minimizing it while there is no common method for leakage detection in this scale for the whole machine, was a challenging project. To minimize the leakage, almost all the connections are replaced and sealed with special sealing materials. Also part of the leakage was because of the gas leakage through the rubber sleeve to the oil chamber and was stopped by using Teflon tubing or aluminum foil around the core samples. The final gas leakage rate for the whole machine was reported 0.35 psi/hr which is reasonable.

- **Data Acquisition:**

There was a serious problem with data acquisition system. It was noted that the data acquisition system doesn't record the pressure values in the right

assigned time step. For example, the system records every 2 seconds when it is assigned to record every 1 second.

To solve this problem and to deal with data sampling and data reduction analysis, a new file was developed in Mathematica®. The developed file gets the raw data from data acquisition system, deals with different time recording steps (since we may use different time steps during the test such as 0.1, 1 and 10 seconds recording interval after the test begins), corrects the time interval for the input data, asks for number of the samples and prepares the sample file regardless of the number of raw data. Assume that we would like to have 100 data points as the representatives of over 25000 data points. The program uses log-log sampling method to choose the best values. For the representative values where there is no direct value in the recordings (for example, we have recorded the pressure values in 10 and 12 seconds and now want the pressure at 10.5 second) linear interpolation between two values was used to estimate the pressure in the unknown times. The output of the Mathematica file is an excel file which can be used at history matching program.

- **Confining Pressure System:**

The electrical-hydraulic pump was used to build up the confining pressure around the core sample. The problem was that the pump was so powerful that it used to build up the confining pressure from 0 to 5000 psi in a few seconds. There were at least 3 problems with this pump:

- The pressure build up rate was too fast and would damage the core
- The pump was strong and could cause safety problems
- It was not practical to set the confining pressure at desired values due to fast build up rate.

To solve these problems, the pump was replaced with a manual and controllable one. It enables us to study stress dependent permeability analysis

- **Use of Different Gasses:**

In this machine, Helium was used for applying the system and pulse pressures. However, there are two important issues that should be taken into account while using Helium:

- Helium molecule is one of the smallest gas molecules in the nature. The inert behavior of this gas and its tiny size makes it easy to leak from any sealed system and not to be detected. So the leakage rate may increase by using Helium.
- Since Helium molecule is much smaller than Methane (as of dominant molecule in natural gas) and of course oil molecules, during the pulse permeability tests, it can be stored in micro pores that in fact neither methane nor oil molecules can be stored there. So it may show permeability and porosity values that are not realistic.

To get reasonable porosity and permeability results and on the other hand to decrease the leakage rate in the machine, the gas was changed to Argon.

Argon has almost similar molecular diameter with methane with a difference in non-toxicity and being inert just like helium.

Two separate modules are added to the history matching program for Argon and Argon gasses. Now the history matching program can analyze tests with Argon and Nitrogen in addition to Helium.

- **Using Core Samples with Different Sizes:**

The machine was developed for 1.5 inch diameter core samples but the problem is that this size of core diameter is not common in petroleum industry and on the other hand some of the core samples are already cut in smaller size and cannot be re-cored. For example to solve this problem for 1 inch diameter samples, rubber spacers are made to fill up the gap between the core holder and the core sample and the appropriate adjustments are made in history matching program.

VITA

Name: Vahid Serajian

Address: Department of Petroleum Engineering,
3116 TAMU- 507 Richardson Building, College Station, TX 77843

Email Address: Vahid.Serajian@Gmail.com

Education: B.S., Mining Exploration Engineering, Amirkabir University of Technology (Tehran Polytechnic), 2006

M.S., Rock Mechanics Engineering, Amirkabir University of Technology (Tehran Polytechnic), 2008

M.S., Petroleum Engineering, Texas A&M University, 2011